TECHNISCHE UNIVERSITÄT WIEN

Master Thesis

Pulse Wave Decomposition and Analysis in Diabetic Patients using Gaussian Peak Fitting

Submitted in partial fulfillment of the requirements for the degree of

Master of Science

Supervised by

Ao.Univ.Prof. Dipl.-Ing. Dr.techn.
Eugenijus Kaniusas

Univ.-Ass. Dipl.-Ing. Stefan Kampusch

to the research group Biomedical Sensors

Institute of Electrodynamics, Microwave and Circuit Engineering

TU Wien

by

Sebastian Schwarzenberger

0707273

Ziegelofengasse 37

2120 Wolkersdorf

Vienna, September 2015

_____

Sebastian Schwarzenberger

Technische Universität Wien

A-1040 Wien • Karlsplatz 13 • Tel. +43-1-58801-0 •

TECHNISCHE UNIVERSITÄT WIEN

Ich erkläre, dass ich meine Diplomarbeit nach den anerkannten Grundsätzen für wissenschaftliche Abhandlungen selbstständig ausgeführt habe und alle verwendeten Hilfsmittel, insbesondere die zugrunde gelegte Literatur, genannt habe.

Weiters erkläre ich, dass ich dieses Diplomarbeitsthema bisher weder im In- noch Ausland (einer Beurteilerin/einem Beurteiler zur Begutachtung) in irgendeiner Form als Prüfungsarbeit vorgelegt habe und dass diese Arbeit mit der vom Begutachter beurteilten Arbeit übereinstimmt.

Wien, im September 2015

Sebastian Schwarzenberger

Abstract

Diabetes induced complications like peripheral vascular disease (PVD) and neuropathy promote the formation of wounds and lead to impaired wound healing in diabetic patients. Early detection and effective, low cost treatment options are key factors to improve the patient's quality of life as well as to reduce health care costs.

New therapeutic approaches like percutaneous auricular vagus nerve stimulation (aVNS) promise to reactivate the autonomous nervous system (ANS), promote wound healing or prevent the formation of new wounds. To monitor the effects of aVNS on the ANS, the pulse plethysmography (PPG) signal of healthy and diabetic patients was recorded and analyzed in the course of a pilot study.

Parameters of interest were the systolic-diastolic volume deflection, the reflection time and the reflection index. For the latter two, the respective incident and reflected pulse waves in each cardiac cycle need to be extracted from the PPG signal. This was achieved by Gaussian peak fitting, using an iterative least-square fitting algorithm. The algorithm was validated by the use of artificial and real measured pulse signals. For most regular PPG signals, fitting errors of < 5 % could be achieved. Using appropriate quality control mechanisms, highly automated and accurate analysis is possible. Besides a decomposition of incident and reflected waves, the original PPG signal can also be reconstituted from the Gauss parameters, and thus may help to save memory.

The feasibility of analyzing full datasets from the pilot study was tested. In this analysis, differences between single healthy and diabetic patients could be observed. Thus, the presented method holds potential for diagnostics and a possible monitoring of therapeutic effects. Long-term effects were not assessed and further analysis is necessary.

Kurzfassung

Diabetes und damit einhergehende Erkrankungen des Gefäß- und Nervensystems begünstigen zusammen mit gestörter Wundheilung die Entstehung chronischer Wunden bei Langzeitdiabetikern. Um die Lebensqualität der Patienten zu verbessern und Kosten zu senken sind sowohl eine frühzeitige Diagnose als auch kosteneffiziente und effektive Behandlungsmethoden essenziell.

Neue Therapien wie die perkutane aurikulare Vagus Nerv Stimulation (aVNS) versprechen die Reaktivierung des autonomen Nervensystems (ANS) zu unterstützen, Wundheilung zu verbessern und die Bildung neuer Wunden zu verhindern. Um die Effekte der aVNS auf das ANS zu überwachen wurde im Zuge einer Pilotstudie das Pulsplethysmographie (PPG) Signal von Gesunden und Diabetikern aufgenommen und analysiert.

Untersucht wurden die Parameter systolisch-diastolische Volumen Änderung, die Reflexionszeit und der Reflexionsindex. Für die letzten beiden Parameter war es notwendig die zugehörige Inzidenzwelle und die reflektierte Welle aus den Pulsen der PPG Signale zu extrahieren. Dazu wurden Gaußpulse in das Signal eingepasst, wobei hierfür ein iterativer least-square Fitting Algorithmus zum Einsatz kam. Der Algorithmus wurde mithilfe von künstlich erzeugten, als auch real gemessenen PPG Pulsen validiert. Für die meisten regulären PPG Signale konnten Fehler von < 5 % erzielt werden. Mithilfe von implementierten Qualitätskriterien für die analysierten Pulse ist ein hochautomatisierter und präziser Analyseprozess möglich. Die originalen PPG Signale können aus den gewonnenen Gaußparametern rekonstruiert werden, was dabei helfen kann Speicherplatz zu sparen.

Die Analyse vollständiger Datensätze aus der durchgeführten Pilotstudie wurde auf ihre Machbarkeit getestet. Bei dieser Analyse konnten Unterschiede zwischen Gesunden und Diabetikern festgestellt werden. Die Methode hat Potential für diagnostische Anwendungen und die Überwachung therapeutischer Effekte. Langzeiteffekte wurden nicht analysiert. Es sind daher noch weitere Untersuchungen notwendig.

Table of Content

1 Introduction

Diabetes Mellitus (DM) has grown to become one of the most widely spread diseases within the last decades. With an estimated prevalence of 387 million cases worldwide, many of them undiagnosed, biomedical research is focusing on treatment options more than ever. [1]

The problems associated with DM include damage to the nervous and vascular system. Patients loose sensitivity in their extremities, impairing their ability to sense potentially harmful forces and/or pressure. At the same time, the autonomous nervous system (ANS) is impaired and blood vessels are damaged. These combined factors cause a higher susceptibility for wound formation. Impaired blood perfusion, a dysfunctional ANS and tissue damage lead to the formation of chronic wounds. [2][3]

In many diabetics such wounds appear on the lower limbs, especially the feet, where they are called diabetic foot ulcers (DFU). These DFUs are very hard to heal and represent a huge reduction in the patient's quality of life. Furthermore, they can get infected and thus may lead to limb loss [4]. Todays limited wound treatment options call for a more sophisticated approach to diabetes induced complications. Diabetic neuropathy is suspected to be at the root of many of those complications. The ANS is connected to the immune system and the peripheral blood perfusion and suspected to play a role in wound healing. Therefore, a method to reactivate the ANS might help to develop relatively low cost treatments which can stop diabetic wounds at early stages.

Auricular vagus nerve stimulation (aVNS) has been used in several studies to influence the ANS and may also help to reinstate the sympathovagal balance that is suspected to be disturbed in diabetic patients. [5] Along with the rebalancing of the ANS, the peripheral blood perfusion is expected to improve. To assess the effects of aVNS, several physiologic parameters like systolic-diastolic volume deflection (SDD), reflection time (RT) and reflection index (RI) can be used. Relative changes in these indices allow to monitor changes in the vascular tone and blood pressure of the patient, and therefore the ANS activity and the peripheral blood perfusion.

In a pilot study, electrical aVNS was used to reactivate the ANS. 10 healthy and 10 diabetic subjects, suffering from DFU, were stimulated using a stimulation device developed at the Research Group Biomedical Sensing at the TU Wien. For the future evaluation of the above parameters, the patient's pulse plethysmography (PPG) signal needs to be analyzed.

This thesis focusses on the implementation of a Gauss fitting algorithm to decompose the digital volume pulse (DVP) waves from the PPG into its incident and

reflected waves. Their timely offset and relative difference in amplitude were then used to calculate RT and RI.

The first section of this thesis gives an overview on the nervous system, the physiological parameters of interest and on diabetes. Subsequently, assessment and processing of the acquired biosignals are described. The indices used for monitoring and the implementation of the Gauss fitting algorithm are explained. The algorithm is validated and finally applied on study data. Example analyses for single measurements are displayed, showing SDD, RT and RI. The results are discussed in detail with respect to the background of this study. The usefulness of the method is assessed and future improvements are discussed.

2 Theoretical Background

2.1 Physiological Basics

2.1.1 The Nervous System

The human body uses two different ways of internal signaling. One is the use of hormones, which are released in one organ to signal its condition or needs to the rest of the body. The effects are generally systemic and relatively slow. The second pathway is the use of nerve cells. These cells form a complex network throughout the whole body and enable signaling with very specific intensities to and from specified organs. They are made up of the cell body and long axons spreading from the cell body to reach organs or other nerve cells. The signals sent by the nervous system (NS) are of electrical nature and, depending on the structure of the nervous pathway, can travel with speeds of up to 120 m/s. [6]

To generate and conduct the signals, the cells use the electrical potential between the inside and outside of the cells. The cell membrane, a phospholipid bi-layer, acts as an isolator. Ion gradients across the cell membrane cause a resting membrane potential of about -70 mV. Special trans-membrane proteins (“sodium-potassium pumps”) continuously pump 2 positive potassium ions into the cell and 3 positive sodium ions out of the cell per pump cycle, conserving the diffusion gradient. This is an active pumping process, where adenosine triphosphate (ATP), the body’s primary cellular carrier of energy, is hydrolyzed. In case of excitation, which can be caused by a physical stimulus as well as by hormones or other external triggers like induced electrical fields, the resting potential is disturbed up to a critical threshold. When this happens, ion channels through the cell membrane open and an action potential (AP) is triggered as described in Figure 1. [6]

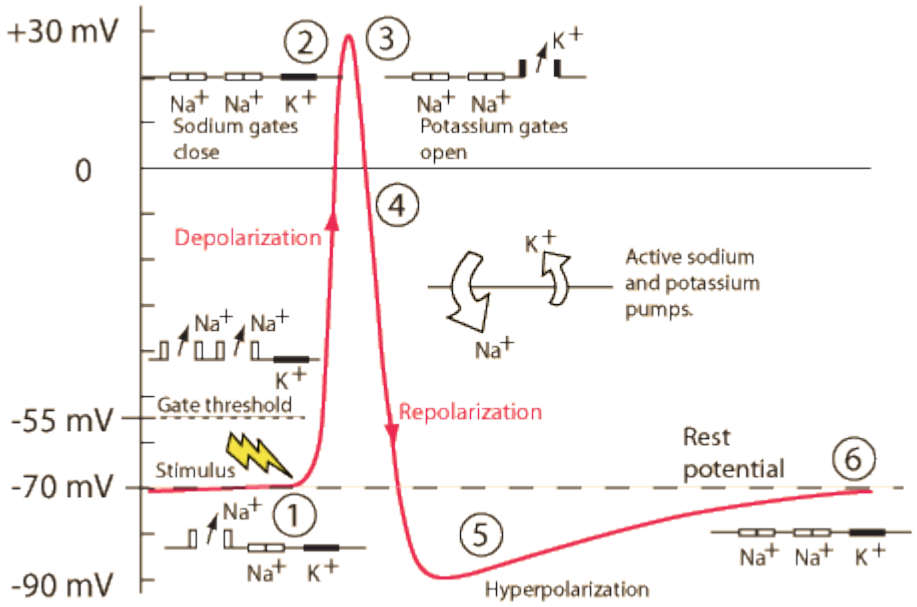

Figure 1: Membrane potential during an action potential, caused by the opening and closing of ion channels. [7]

The ions mainly pass these channels because of their concentration gradient in- and outside the cell membrane, not because of their charges. However, the charges carried by the ions influence the membrane potential, which peaks around 50 mV. After excitation, the resting potential is restored, because potassium ions leave the cell through K^+ channels. Potassium and sodium ions are now located on the wrong side of the cell membrane. In this phase, the refractory phase, excitation is not possible while ions are being pumped back to their respective sides by the sodium-potassium pumps.

An AP however is only a snapshot from one particular spot on a nerve cell. In order to transmit the signal, APs have to be forwarded along the membrane. This is enabled by the fundamental characteristics of the electrical field. The AP causes equalizing currents and disturbs the resting potential in surrounding areas of the originally excited spot as well. There, the threshold for excitation may be reached and another AP can be triggered. In this fashion, the signal spreads from the originally excited spot.

Nervous signal transmission of this kind is the simplest one and is also relatively slow with speeds of ~1 m/s, depending on the diameter of the axon. To speed up transmission, many nerve cells have axons with Schwann cells wrapped around. These act as an insulator and allow for the axon's membrane only to be excited at those locations, where the Schwann cells leave a small gap in between each other. The equalizing currents of an AP can bridge the distance over a Schwann cell, but without needing to cause APs all the way in between. Transmission speeds of up to 120 m/s can be achieved in the human body this way.

Autonomic Nervous System

The nervous system can be divided into anatomic and functional subdivisions as shown in Figure 2. Especially interesting for therapeutic application is the autonomic nervous system (ANS) which is responsible for involuntary processes in the body.

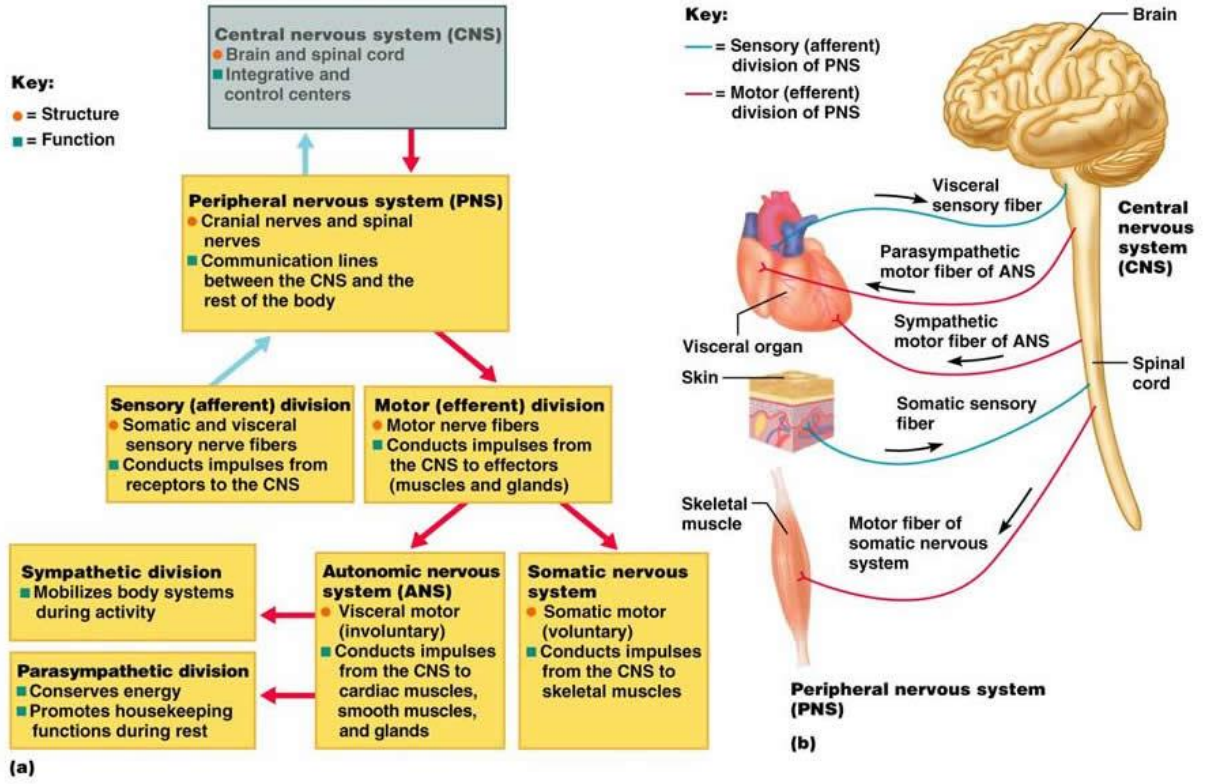

Figure 2: Structural and functional setup of the nervous system, including the ANS. [8]

These processes include regulation of heart beat, body temperature, blood pressure and others. It is further split up into the sympathetic and parasympathetic nervous system, working in an antagonistic fashion to keep the body as active as necessary (sympathetic) while conserving as much energy as possible (parasympathetic). The sympathetic system stimulates fight-or-flight responses, it elevates heart rate and blood pressure. The sympathetic system also regulates the vascular tone of arteries by innervation of the smooth muscles surrounding them. An increased sympathetic tone leads to vasoconstriction, yielding stiffer arteries. [9]

The parasympathetic system is dominant in so called rest-and-digest situations, reducing heart rate and blood pressure and also regulating inflammatory responses. [10][11]

Vagus Nerve

One integral part of the parasympathetic system is the tenth cranial nerve or vagus nerve (VN). Its name is derived from the Latin word for “Wanderer”, because the nerve is so widely spread throughout the whole body, connecting various organs to the central nervous system (CNS). About 80 % of the VN are afferent fibers, delivering information to the CNS. The VN is therefore considered a relatively easy-to-reach gateway to the brain and influences major physiological processes. The VN has been described to play an augmenting role in inflammatory responses [12] and as an interface between the nervous system and the immune system. [13]

2.1.2 Physiological Parameters

ECG

Just like any other muscle, the heart muscle needs innervation to contract in an orderly and regular fashion. It consists of two different functional units, the ventricles and the atria, which contract successively to pump the blood through the circulatory system.

The atrial and ventricular muscle are separated by an insulating layer of tissue to allow for coordinated electrical excitation. The progressing excitation can be monitored using electrodes on the skin to follow the heart’s electrical dipole vector. A standard method to place these electrodes on the patient is the Einthoven I derivation, where they are put on the left and right shoulder or wrist. A regular heartbeat then yields the electrocardiogram (ECG) depicted in Figure 3.

Initial excitation takes place in the sinoatrial node where it starts spreading over the atria, forcing them to contract and fill the ventricles with blood. Since the atria are insulated from the ventricles, excitation can only continue through a nervous pathway penetrating this insulation. Over the atrioventricular (AV) node and the HIS bundle it reaches the ventricles and forces them to contract and to eject the blood into the circulatory system. The three nodes/bundles act as pacemakers for the heart and have specific frequencies. One node can take over if the preceding one fails. The specific frequencies are, in order of their priority; ~70 BPM (sinoatrial), ~50 BPM (AV), ~30 BPM (HIS). The different phases of a heartbeat with corresponding ECG events are described in Figure 3.

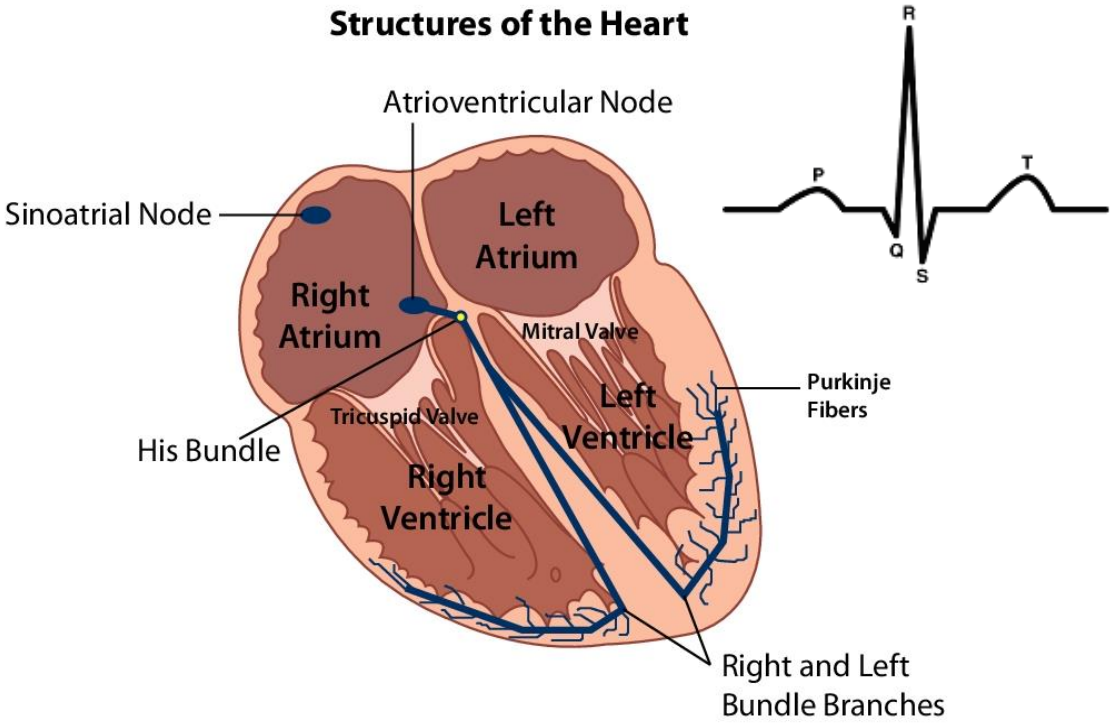

Figure 3: Scheme of the heart's electrical and functional structure with a standard Einthoven I ECG. P-wave: Excitation spreads over atria. PQ-segment: Maximum excitation of atria. QRS-complex: Excitation spreads over ventricles, following the nervous pathways (blue). Repolarization of the atria is hidden by this more prominent process. ST-segment: Maximum excitation of ventricles. T-wave: Repolarization of ventricles. [14]

As shown in Figure 4, the regular system of electrical excitation in the heart can fail and cause extra contractions of the whole or parts of the heart. These extra contractions are called extrasystoles.

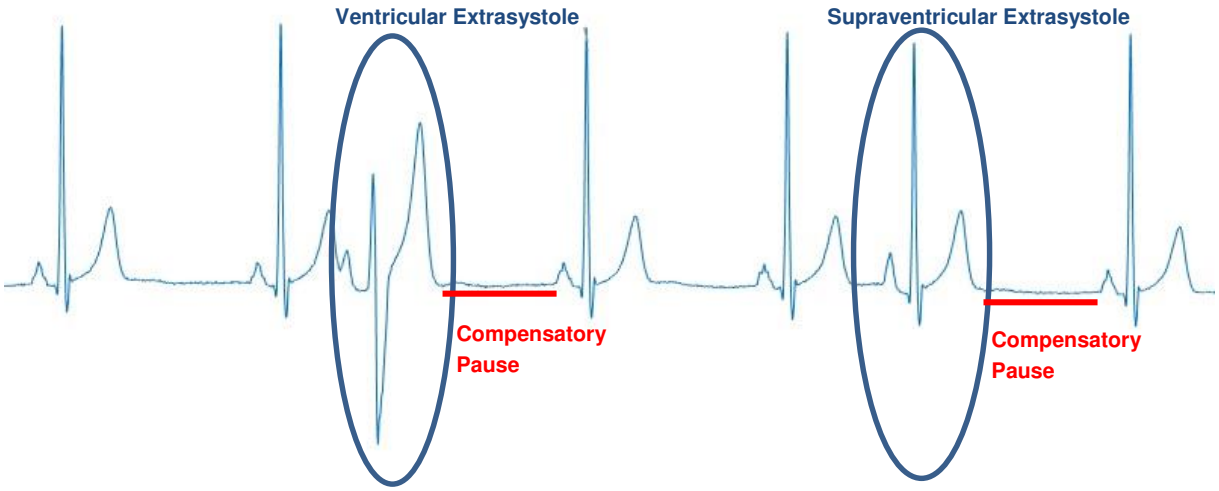

Figure 4: ECG showing two types of extrasystoles.

In general, any excitation of the heart muscle originating anywhere but the pace making nodes is called extrasystole. However, form and consequence of an extrasystoles are primarily dependent on its origin. They are roughly divided into two groups.

If an irregular excitation happens anywhere in the atrial region, it is called a supraventricular extrasystoles. Excitation will include the atria and then be further directed to the ventricles. The heartbeat will look like a regular one in the ECG, but appears earlier than expected and shows a slightly altered P-wave.

If an irregular excitation happens in the ventricular region, only the ventricles will be affected and contract without having been filled by the atria before. The ECG in this case looks very different (Figure 4) and these ventricular extrasystoles are usually perceived by patients as “skipped beats”. Both types of extrasystoles are usually followed by a compensatory pause, allowing the system to fall back into its regular cycle.

For ECG analysis, the possible occurrence of extrasystoles has to be kept in mind. They disturb calculations of heart rate (HR), heart rate variability (HRV) and other evaluations, since they do not represent the regular pulse as given by the body’s regulatory mechanisms.

Pulse Wave

The human circulatory system can be separated into a high pressure part and a low pressure part. The high pressure part with an average of 100 mmHg contains the arterial network. It delivers oxygenated blood to the capillaries and serves as the supplying framework to the body’s consumers. The low pressure system, made up of the venous system with an average of only 15 mmHg contains about 80 % of the blood. It allows the blood to flow back to the heart and also serves as a reservoir.

In the course of one pulse cycle, vessels are subjected to pressure changes. To allow for effective blood flow the ANS causes them to constrict and dilate continuously. The vessel walls and surrounding tissue are subject to aging, causing this process to become less effective in the course of a lifetime. This process can be accelerated by diabetis mellitus (DM) and the implied glycation (see 2.2.2). The result are stiffer walls and a shift in the sympathovagal balance where vagal activity decreases, impairing vessel relaxation and inhibiting the vessel’s regulatory functions.

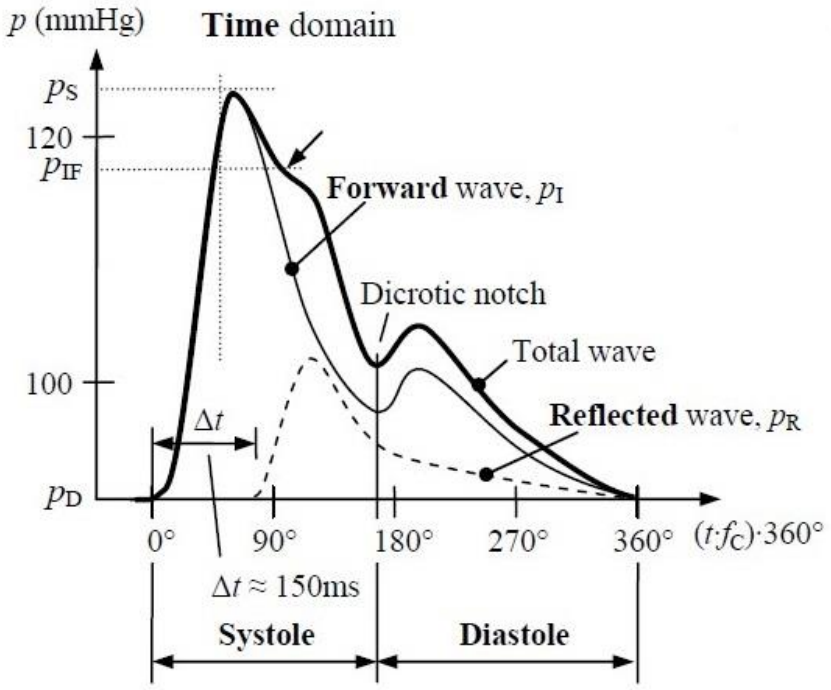

Figure 5: Schematic of a human pulse wave. Δt is the round trip time of the pulse wave from the heart to the reflection site and back [9]

The condition of a patient's cardiovascular system can be monitored using pulse plethysmography (PPG). Figure 5 describes what a regular pulse wave looks like and how it is composed of not only the initial pulse caused by the beating heart, but also overlapping reflections of this wave, forming a classic pulse wave. However, the pulse waves recorded by PPG are not actual pressure waves, but digital volume pulse (DVP) waves. They carry similar information, and have a similar appearance, but are based on the blood volume passing through the monitored vessels.

Older or damaged vessels with higher stiffness lead to shorter travel time and less damping of the pulse wave. The reduction in Δt and a stronger reflected wave can lead to a super elevated total wave, putting higher loads on the heart and further damaging vessels. Except for muscular arteries, arteries in the lower body experience a greater degree of stiffening. This is a fact that is all the more problematic, since the smaller vessels should usually maintain a steadier blood flow to ensure continuous blood support of organs and tissue. This continuous flow is enabled by the Windkessel effect; elastic arteries store and release blood to even out the pulsatile components. Since the Windkessel effect is based on dilatable arterial walls, the blood flow in smaller vessels is still pulsatile in diseased people due to stiffer walls. In elderly diabetics this pulsatile wave may result in tissue damage, because tissue located next to small vessels is usually not adapted to discontinuous blood flow. This condition, known as Peripheral Artery Disease (PAD) ultimately leads to necrosis and the formation of Diabetic Foot Ulcers (DFUs).

Vascular disease and the causes of diabetic wounds are directly linked to the functionality and structure of the human circulatory system, making it important to understand the underlying physiological principals.

2.2 Diabetes Mellitus and its Consequences

DM is a group of metabolic diseases which is characterized by a dysregulation of the body's insulin equilibrium. The resulting chronic hypoglycemia is associated with long-term damage, dysfunction and failure of different organs, especially the eyes, kidneys, nerves, heart, and blood vessels. Complications include cardiovascular diseases, stroke, microangiopathy and peripheral vascular disease (PVD). Figure 6 illustrated the prevalence of DM worldwide.

Two basic forms of DM are distinguished. Type 1 diabetes is caused by an absolute deficiency of insulin secretion and type 2, which is way more prevalent, originates from a combination of resistance to insulin and an inadequate compensatory insulin secretion response.[15]

DM has grown to become one of the most widely spread diseases within the last decades. With an estimated prevalence of 387 million cases worldwide, many of them undiagnosed, biomedical research is focusing on treatment options more than ever.[1]

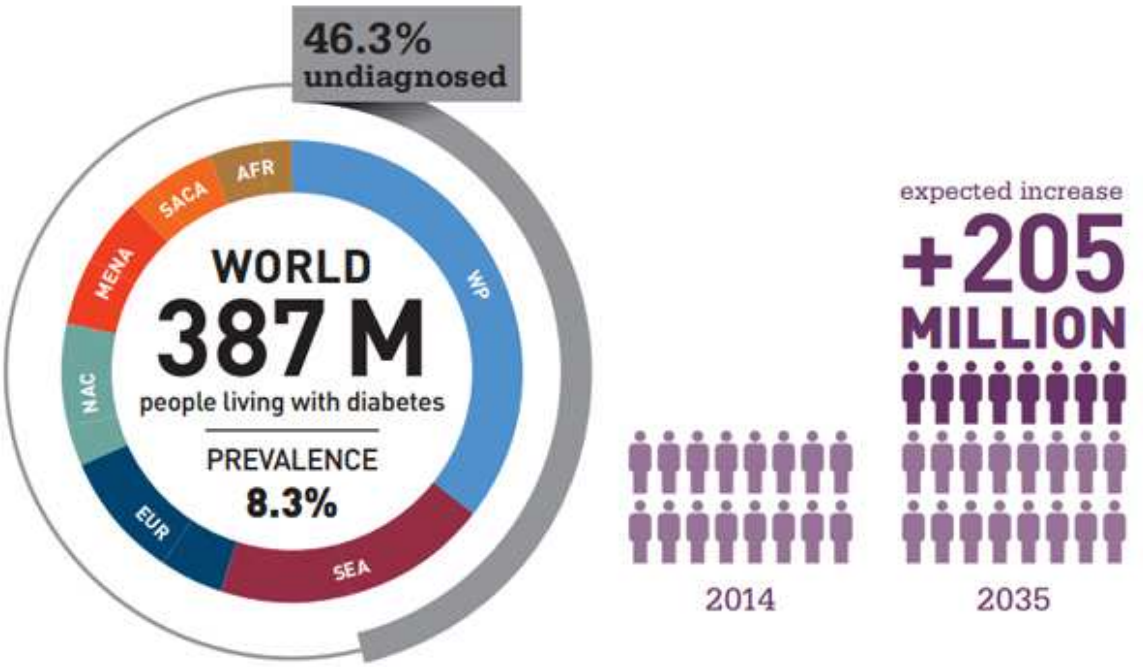

Figure 6: Prevalence of diabetes worldwide: Western Pacific (WP), South East Asia (SEA), Europe and Russia (EUR), North America and Caribbean (NAC), Middle East and North Africa (MENA), South America and Central America (SACA), Africa (AFR) [1]

2.2.1 Type 1 & 2 Diabetes

Type 1 diabetes, known as juvenile-onset diabetes, is usually caused by an auto-immune reaction. The immune system attacks pancreatic β-cells that produce insulin. The reason for this is not fully understood. A variety of exogenous factors seem to play a role in the development though. The Hygiene Hypothesis suspects increased hygiene and better living conditions as a promotor to auto-immune reactions. Other causes may be a patient's genotype, socioeconomic status, obesity, early infant nutrition, prenatal exposure to organochloride pollutants and low vitamin D levels.

People with type 1 diabetes produce very little or no insulin. The disease may affect people of any age, but usually develops in children or young adults. People with this form of DM need injections of insulin every day in order to control the level of glucose in their blood. [16]

The second and much more prevalent form of DM is type 2. Formerly known as non-insulin dependent diabetes or adult-onset diabetes, it accounts for at least 90 % of all cases of DM. It is characterized by insulin resistance and relative insulin deficiency, either of these conditions or both may be present at the time DM is diagnosed. Type 2 diabetes may develop at any age. It may remain undetected for many years and the diagnosis is often only made when a complication appears or a routine blood or urine glucose test is done. It is often, but not always, associated with overweight or obesity, which itself can cause insulin resistance and lead to high blood glucose levels. An absolute criterion for the diagnosis of DM is a blood plasma glucose concentration of ≥ 200 mg/dl. In healthy patients this value is typically about 80 mg/dl. People with type 2 diabetes can often initially manage their condition through exercise and diet. However, over time most patients will require oral drugs and/or insulin. [16] Table 1 lists the main features and differences between type 1 and type 2 diabetes.

Feature	Type 1 diabetes	Type 2 diabetes
Onset	Sudden	Gradual
Age at onset	Mostly in children	Mostly in adults
Body size	Thin or normal	Often obese
Ketoacidosis	Common	Rare
Autoantibodies	Usually present	Absent
Endogenous insulin	Low or absent	Normal, decreased or increased
Prevalence	~10 %	~90 %

Table 1: Key Features of type 1 and 2 diabetes. [17]

2.2.2 Complications

The constantly high glucose levels associated with DM create complications on a cellular level which can lead to long term damage and impairment of bodily functions, especially in the vascular system.

Hyperglycemia promotes the formation of covalent adducts between glucose and plasma proteins through a non-enzymatic process known as glycation. Typical binding partners are plasma proteins like albumin, fibrinogen and globulins or collagen. Glycation leads to impaired protein function, the formation of free radicals, inflammation and in succession to neuronal and vascular dysfunction (Figure 7).

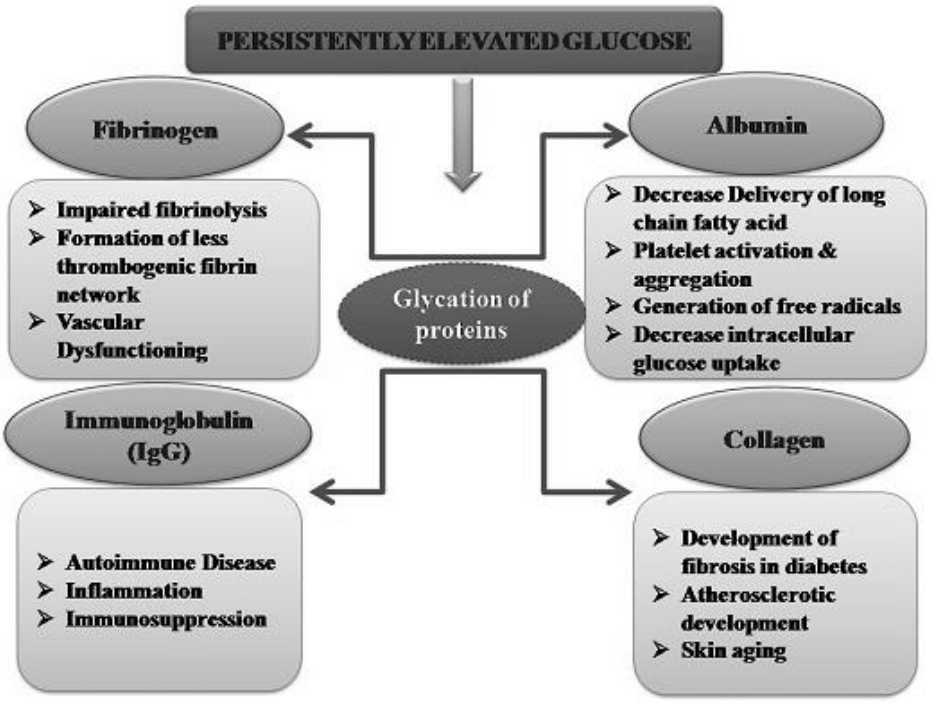

Figure 7: Long term effects of glycation on a cellular level. [18]

Glycated proteins can undergo further reactions, giving rise to poorly characterized structures called advanced glycation end products (AGEs). These AGEs can lead to inflammation or occlusion in the vascular system, primarily affecting small vessels found in the retina, nephrons or of peripheral arterioles/venoles. They are believed to cause most vascular related complications in diabetic patients like retinopathy and cataract.

Furthermore, the glycation of Schwann-cells causes segmental demyelination and axonal degeneration of peripheral neurons, leading to reduced signal conduction and impaired sensory function. Combined with the vascular dysfunction, this diabetic neuropathy does not only increase the risk of tissue damage and necrosis, but also promotes decreased wound healing abilities which are linked to autonomous nervous systemic action. [18]

For some DM induced vascular complications like retinopathy and nephropathy, standard therapies have been successfully developed and are already applied in the clinical routine. Others however remain a huge challenge for biomedical research.

Vascular diseases can be roughly classified in two groups; macro- and microangiopathy. Macroangiopathy can cause heart attack, stroke and PVD, while microangiopathy may cause the formerly mentioned nephropathy, retinopathy and neuropathy. [2]

Combined with the decreased wound healing capabilities, the increased risk of tissue damage promotes the development of chronic wounds in diabetic patients. These wounds usually appear in pressure points of the lower extremities, especially the feet, where so called Diabetic Foot Ulcers (DFU) occur. Approximately 4.1 % of diabetic patients develop such a DFU each year, resulting in a lifetime incidence of 25 %. Even with standard care, about 1 % of diabetic patients have to undergo amputation of lower extremities every year, making DM the leading cause of non-traumatic amputation. [3]

Diabetic Foot Ulcers and Diabetic Foot Infections

The polyneuropathy and PAD associated with DM may lead to the development of DFUs. A DFU is any full-thickness wound below the ankle in a diabetic patient, irrespective of duration. Approximately 58 % of DFU patients will become clinically infected and develop a diabetic foot infection (DFI). DFI treatment accounts for up to one-quarter of all diabetic admissions in both Europe and the United States making it the single most common reason for DM-related hospital admission. In the longer term, costs are even higher as DFUs have recurrence rates of up to 70 %, resulting in repeated interventions and progressive disability. Even with the best therapy and preventive care, 9 % of all DM patients develop a DFI with the consequent risk of amputation [4]. Figure 8 illustrates which roles the different risk factors caused by DM play in the development of DFUs and DFIs.

To avert the excessive costs and loss of quality of life going along with DFI and amputation (Figure 9), clinical procedures for DFU management need to be improved. The most interesting approaches aim at early stages of the disease where the damage is still minor and therapies should help the patient to live as unaffected as possible by the implications of DM. For early detection of risk factors for DFUs and diabetic wounds, the condition of a patients vascular and nervous system needs to be monitored with as little effort as possible.

One possibility for relatively uncomplicated monitoring is the analysis of the patients pulse wave. Especially methods for analysis of PPG signals were reviewed and developed in the course of this thesis. Implemented algorithms were tested with real

data from measurements during the application of a new treatment modality, the so-called auricular vagus nerve stimulation (aVNS).

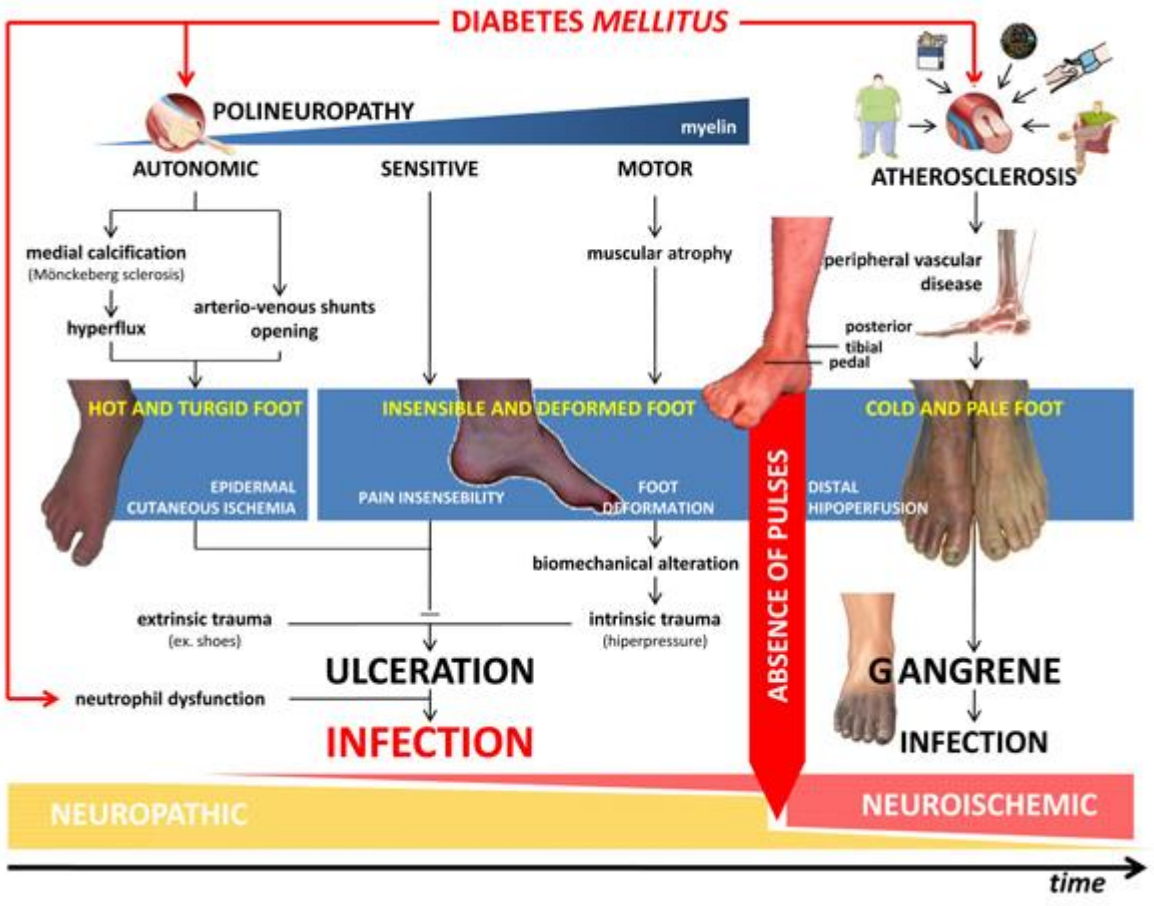

Figure 8: DFU and DFI pathophysiology. DFU results from a complex interaction of a number of risk factors. Neuropathy (with alterations in motor, sensation, and autonomic functions) plays the central role and causes ulcerations due to trauma or excessive pressure in a deformed foot without protective sensibility. Once the protective layer of skin is broken, deep tissues are exposed to bacterial colonization. Infection is facilitated by DM-related immunological deficits, especially in terms of neutrophils, and rapidly progresses to the deep tissues [4]

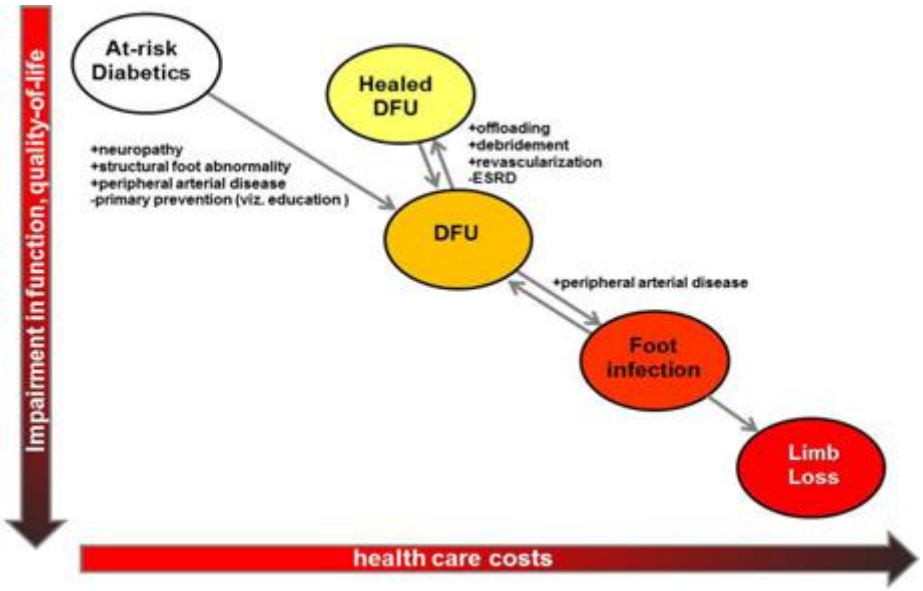

Figure 9: The clinical states leading to limb loss among patients with DM and the risk factors that influence the transition between these states. [19]

2.2.3 Therapy

Aside from obvious therapeutic approaches like glycemic control, patient education and wound care, there have been interesting advances in diabetic wound management. These include the development of new wound dressings, growth factors, bioengineered skin and tissue substitutes, hyperbaric oxygen, negative pressure wound therapy and other novel approaches to stimulate wound healing. Many of these approaches were proven to be effective for wound management and healing. However, effectiveness is limited, they are expensive, and address the problem at a stage where wounds have already formed and are prone to infection.

Despite these advances, it is therefore important to remember the fundamental basics in controlling diabetic foot ulcers: adequate perfusion, debridement, infection control, and pressure mitigation to allow skin and tissue regeneration instead of scar tissue formation. [3]

Electrostimulation

A different, simple and relatively cheap alternative approach to diabetic wound management is electrostimulation (ES). A study [20] has used electrical pulses to stimulate intact nerves in the affected wound area to promote perfusion and achieved enhanced healing rates by nearly 60 % over the control group. However, another study [21] criticized the pool of patients in this trial, since diabetics with evidence of PVD were excluded. This second study was a pilot study which investigated ES with a randomized pool of diabetics. ES was applied subsidiary during a phase of intense wound care and pressure relief. The results suggested strongly improved wound healing, also in patients with PVD.

It seems that improved wound healing through ES is mainly due to enhanced vascular activity and perfusion. [22] This effect on the vascular system is not surprising, since diabetic patients usually suffer from neuropathy and PAD, leading to wound formation and impaired healing. ES may substitute or support regular nervous control and promote healing.

Auricular Vagus Nerve Stimulation (aVNS)

Although impressive, the effects of ES are local and do not help to regenerate nervous tissue damaged by neuropathy. From a systematic perspective, influencing the activity of the ANS means to influence the body's regulatory capacities. Such an approach aims to move from local interventions like ES to systemic regeneration where tissue damage and wound formation is not only treated, but prevented on the long-term.

Wound healing is influenced by the ANS and is dependent on its regulatory function. In neuropathic diabetics it is suspected that the damaged NS experiences a misbalance, shifting the working point into a region where effective regulation of perfusion and inflammatory response is no longer possible. The idea behind vagus nerve stimulation (VNS) is to bring the ANS back into a balanced state, thus allowing the body to (partially) regain control (Figure 10).

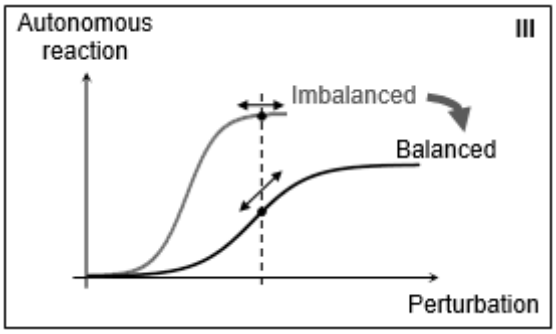

Figure 10: An imbalanced ANS has very limited regulatory scope. aVNS may help rebalancing it. [23]

The reason why especially the VN is stimulated lies in its anatomical and functional properties. From a functional point of view, it is suspected to act as a link to the immune system, where it regulates inflammatory responses [12][13]. Established applications of aVNS are seizure control in epilepsy [24], mood disorders [25], chronic cervical pain [26], chronic low back pain [27] and PAD [28]. It has also been shown that aVNS affects HRV and blood perfusion [5] making it a vital part of the parasympathetic NS in terms of regenerative functionality and wound healing. The described achievements have made the VN a promising target for research, since the precise effects of VNS on the human body remain undisclosed. Local and systemic effects of VNS can probably be detected in many more critical parameters for wound healing and tissue regeneration and remain to be investigated.

The VN consists of 80 % afferent fibers and is therefore predestined to act as a gateway to regulatory control loops in the NS. The auricular branch of the VN allows easy access to these structures. The nerve fibers usually run in parallel to the superficial vessels in the auricle which can easily be detected using impedance measurement or visual inspection. Percutaneous electrodes can easily be applied in a minimally invasive procedure, making aVNS safe and effective.

3 Pulse Wave Analysis

For this thesis, a Gauss fitting algorithm was implemented and tested for the decomposition and analysis of DVP curves which were taken from PPG signals.

The data of an open, randomized, prospective and monocentric pilot study was used for evaluation of the implemented algorithms. The study was designed to investigate the effects of aVNS on critical parameters for wound healing in chronic diabetic wounds, especially DFUs.

Two groups of patients were included in the study. Group 1 (n=10) consisted of diabetic patients with chronic wounds (Ulcus Cruris) and group 2 (n=10) consisted of healthy subjects.

Combined main goal of the study is an assessment of the stimulation-induced modulation of HRV and blood perfusion index (BPI) with respect to their initial state. It is expected that modulation in diabetic subjects suffering from a chronic disease will be more prominent, since sympathetic/parasympathetic equilibrium is shifted to sympathetic activity in these patients. aVNS is expected to help rebalance the ANS.

To assess stimulation-induced modulation of the ANS, other physiological parameters are analyzed as well. This includes investigation of the BPI, transcutaneous oxygen tension and especially detailed analysis of the patients pulse wave, recorded with PPG. Approaches to pulse wave analysis are described and validated in this thesis to allow for more accurate analysis in the future.

Parameters discussed in this thesis are systolic-diastolic volume deflection and decomposed incident and reflected waves using a Gauss fitting algorithm. Incident and reflected waves are then further analyzed with respect to their different amplitudes and time offset.

3.1 Setup and Protocol

10 healthy patients and 10 diabetics with DFUs were subjected to electrical aVNS in 4 sessions each. During every session, the patient's vital parameters were monitored and recorded. Some patients also had an extra measuring session before and after the four aVNS sessions to record baseline levels without stimulation. Apart from the missing stimulation, these sessions were identical to the regular ones. It was attempted to conduct the sessions on consecutive days and at the same daytime to avoid the biasing of results.

Every session lasted 84 minutes and included periods with stimulation as well as intermissions without. The precise timetable of one session is depicted in Figure 11.

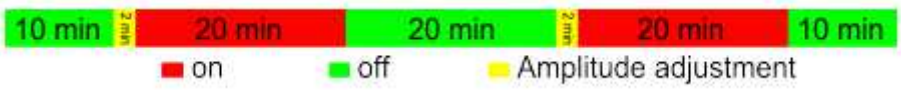

Figure 11: Protocol of one session. Green: Pause (First Pause is Baseline); Yellow: Individual adjustment of the Amplitude; Red: Stimulation.

Out of the 4 sessions with stimulation, 2 used a biphasic stimulation pattern and 2 a so-called triphasic stimulation (Figure 12 and Figure 13). Assignment of the stimulation patterns was randomized.

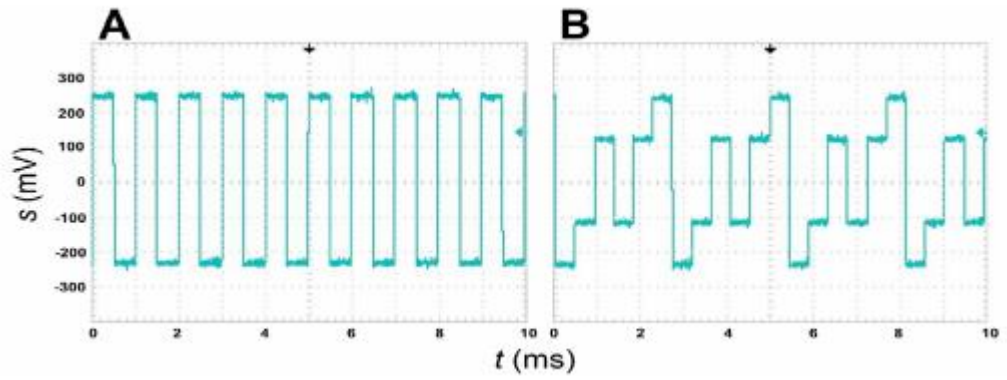

Figure 12: Oszillogram of one channel for biphasic (A) and triphasic stimulation (B).

Figure 13 also shows how the percutaneous auricular needle electrodes were attached to the auricle. The actual positions were determined using resistance measurements in order to locate superficial vessels and thus the vagus nerve.

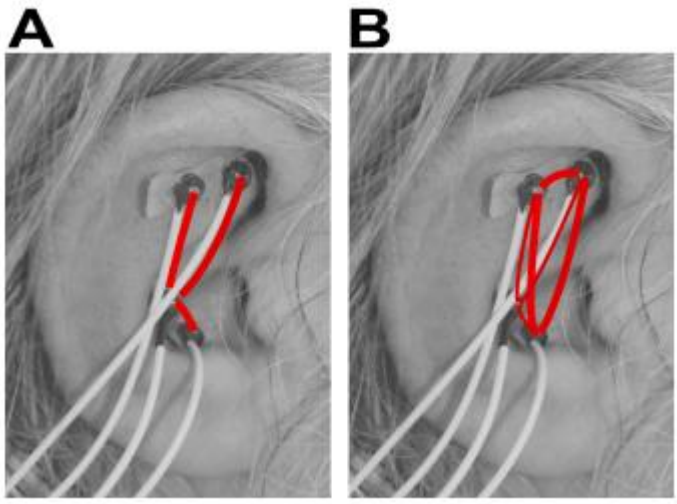

Figure 13: 4 PrimeStim electrodes (3 signal, 1 reference). The red lines show expected current pathways for biphasic (A) and triphasic (B) stimulation.

The electrodes were placed in the auricle before the first session and were not removed until the end of the last session. To avoid artefacts, patients had to lie still during the whole session.

Data conversion, synchronization and analysis was performed in MATLAB® R2014b.

3.2 Assessment of Biosignals

ECG

In this study, the ECG was acquired using an Einthoven I derivation. It was used to synchronize the applied measurement systems. Furthermore, R-peaks mark the beginning of a pulse and are therefore used as reference point for the following analysis.

After synchronization, the ECG signal was analyzed for R-peaks. R-peak detection was performed using a proprietary algorithm [29] which is based on differentiation of the signal, since the primary characteristic of R-peaks is the steepness of the slope.

The result was then displayed in a graphical user interface (GUI) (Figure 14 and Figure 15). To ensure good data quality, the signals had to be checked for correct detection and extrasystoles, which needed to be removed.

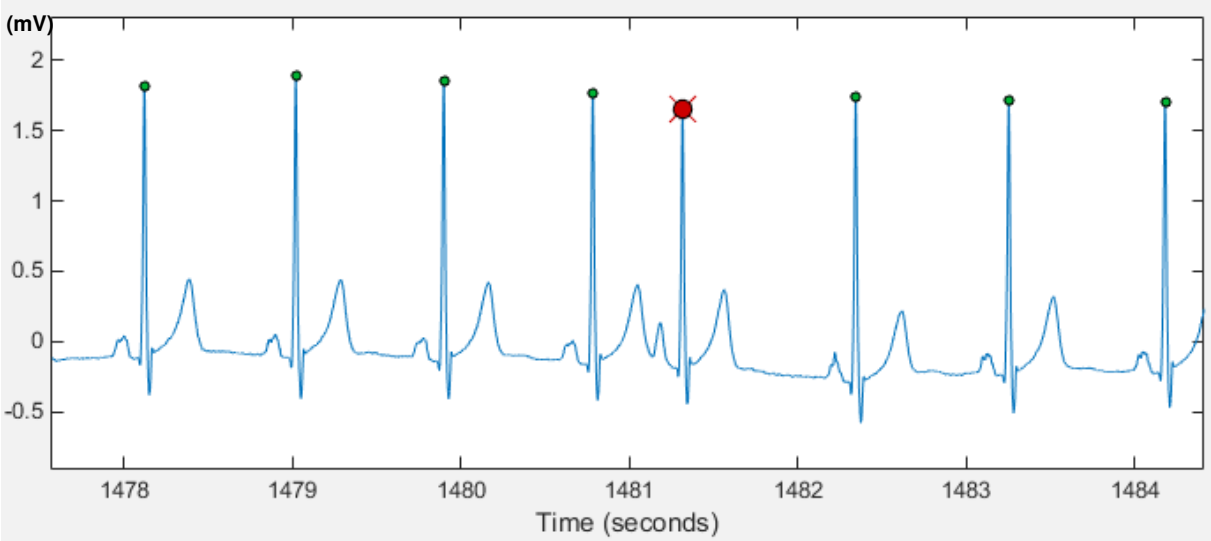

Figure 14: ECG after R-peak detection. R-peaks are marked with a green dot. The green marker on the extrasystole, in this case a supraventricular extrasystole, has already been removed and has been replaced with a red marker.

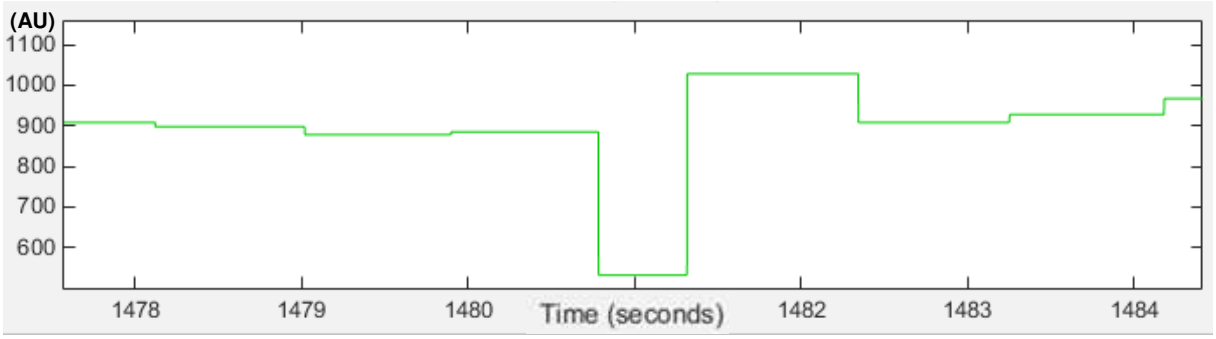

Figure 15: The peak-to-peak interval was displayed in an extra window to allow for easy identification of extrasystole, which usually lead to deflections in the otherwise smooth curve. The deflection shown here corresponds to the extrasystole displayed in Figure 14.

PPG

PPG signals were acquired from the patients left index finger as well as from the big toe. For reasons of signal quality (vasoconstriction regularly obscured and flattened the signal to a point where it became unusable) only the PPG from the big toe is used in this thesis. This signal was recorded using a Nellcor® pulse oximeter which uses an integrated filter and adaptive gain to provide constant signal quality.

After data conversion, minima and maxima in the PPG signals were detected using a proprietary algorithm. Since PPG slopes are not as steep as the ECG signal, differentiation would not have yielded satisfying results. The algorithm was subject to ongoing improvement in the course of the thesis. Since min/max detection was verified visually using a GUI, just like the R-peak detection before, the constant changes in the detection algorithm didn't compromise detection results in the end.

The detection algorithm relies on the previously detected R-peaks to find min/max peaks in the PPG signals. Windows in which the peak is expected were defined and the max/min value of the signal within this window was then detected (Figure 16).

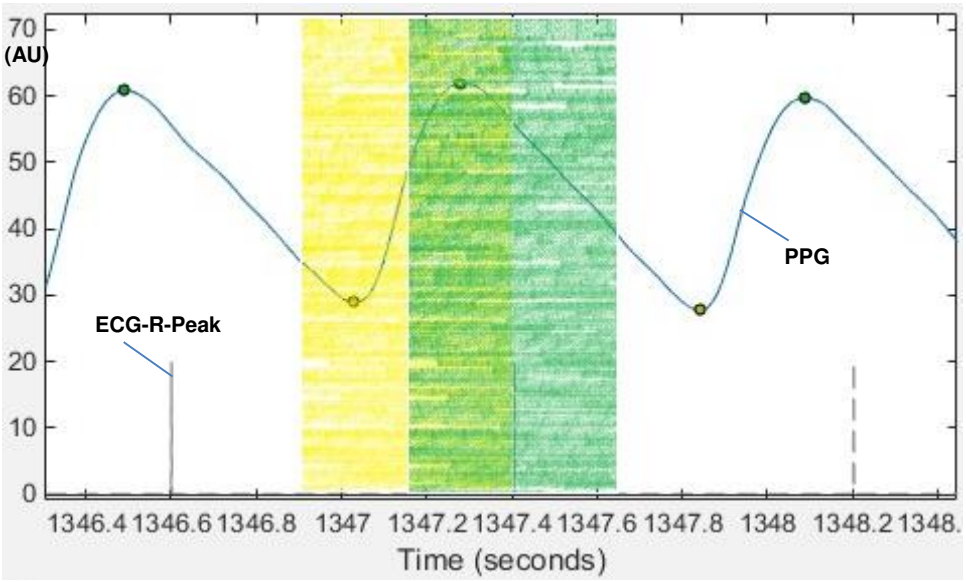

Figure 16: Window for min peak (yellow) and max peak (green). The window for max peak detection was set ±250 ms around the R-peak subsequent to the pulse, while min peak detection was performed in a window of 500 ms before this R-peak. R-peaks are displayed as grey lines.

The windowing method, while simple, also leads to problems that needed to be addressed. The first and most obvious problem was ill-defined windows, which didn't contain the desired peak. Figure 17 depicts how peaks were detected wrongly at the window limits in this case. These peaks could best be identified visually with histogram analysis, since they all showed a characteristic distance to the R-peak.

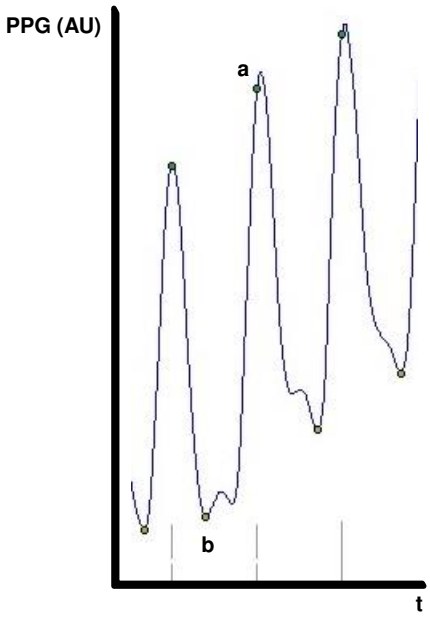

Figure 17: Max peaks which were detected on the border of an ill adjusted detection window (a) and one min peak wrongly detected at the inscision between forward and backward wave, because the signal was drifting (b).

Due to large variations in between the individual patients and the signals themselves, windowing errors could not be completely eliminated and such peaks had to be corrected manually.

A second problem, and also a reason why windows could not be dimensioned arbitrarily, was late reflections, drifts and other influences on the signal which could lead to additional extrema in the signal (Figure 17). The solution was a validating function in the detection algorithm, checking for such typical misdetections.

Another helpful tool was the histogram based visual inspection of pulse arrival times (PATs) (Figure 18). Later in the analysis, PAT analysis was used to remove irregular pulses from the dataset automatically.

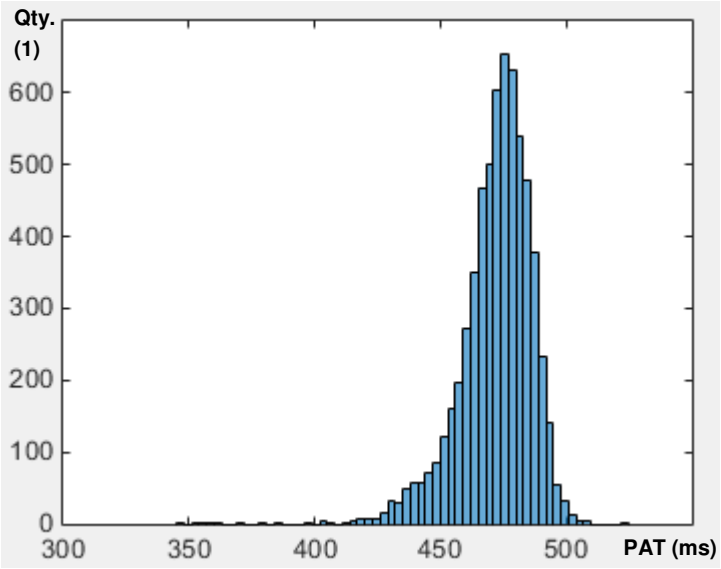

Figure 18: Histogram describing the pulse arrival times (PATs) of all pulses in the signal. PAT is the time elapsed from the ECG R-peak until the arrival of the pulse (PPG minimum peak).

3.3 Signal Processing

After max/min detection, various methods for signal processing were evaluated within this thesis. The PPG signal was analyzed by calculating the systolic-diastolic deflection volume from the already existing min/max peaks data.

Besides simple features extracted by min-max detection, single PPG peaks were tried to be decomposed using Gaussian waves. This should enable the separation of forward and backward waves in the pulse signal.

To this day, methods for pulse wave decomposition do already exist, but they are either expensive (MRI based methods) or not very stable, like the Second Derivative of Digital Volume Pulse (SDDVP), which is currently the standard for analysis of DVP waves. In this method, the turning points in the PPG slope are labeled a, b, c, d and e waves. The relative heights of these waves have been related to age, arterial blood pressure, large artery stiffness and effects of vasoactive drugs [30]. However, the performance of this method will degrade when the DVP signal is weak and noisy, especially when the diastolic part of the DVP waveform monotonically decreases [31].

The fitting of Gaussians and other statistical distributions has already been applied to PPG signals in several other studies. Many of them [31][32] follow Multi-Gaussian fitting approaches and try to more effectively extract feature points (often referred to as a, b, c, d and e waves) from the PPG. Instead of using the second derivative, they directly fit up to seven [31] Gaussians into the PPG, approximating the slope as well as possible.

However, the SDDVP and Multi-Gaussian approaches deliver useful results, they have already moved well away from the original idea of how pulse waves are composed in the physiological environment. One study [33] has tried to disassemble pulse waves into its original forward and backward waves by fitting two Rayleigh functions into the DVP wave. The extracted forward and backward waves were then used to directly assess the condition of the patient's vascular system.

In this theses the PPG signals are decomposed just like in [33], but in this case the forward and backward waves are approximated by Gaussians. The separated waves were then used to investigate further parameters which might show effects of the aVNS. These parameters were the timely offset between forward and backward wave as well as the relative intensity of amplitudes. Both of which may indicate changes in the vascular tone.

3.3.1 Systolic-Diastolic Deflection

The PPG contains information about the blood pressure and vascular compliance of the trans-illuminated vascular bed. The systolic-diastolic volume deflection of the PPG is the difference of the maximum and minimum amplitude of the signal (Eq. 2.1).

$$s_{S,D} = s_S - s_D \tag{2.1}$$

It is proportional to the pulsatile systolic-diastolic blood volume $V_{S,D}$. This pulsatile volume corresponds to the product of the local systolic-diastolic deflection of the blood pressure $p_{S,D}$ and the arterial compliance of the vascular wall (= V/κ with V as the total volume and κ as the module of volume elasticity of the vessel), see Eq. 2.2.

$$s_{S,D} \propto V_{S,D} \approx p_{S,D} * \frac{V}{\kappa} \tag{2.2}$$

In other words, the deflection increases with increasing $p_{S,D}$ and decreasing stiffness of the vessel. However, the module κ, which describes this stiffness, is not constant over the varying blood pressure. It rises with increasing blood pressure, leading to decreased arterial compliance. In other words, the module κ is inversely proportional to the local slope of the relationship between vessel radius and blood pressure (Figure 19) [34].

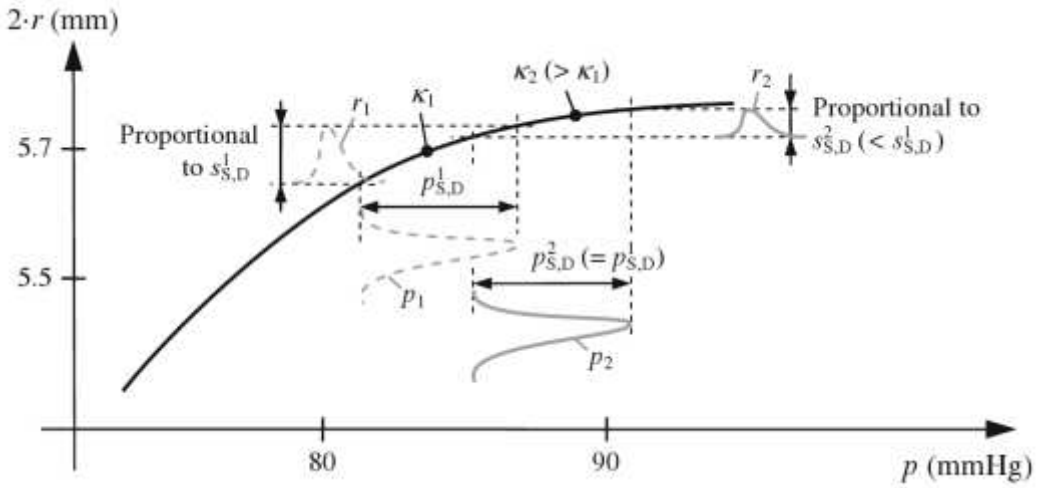

Figure 19: Relationship between blood pressure and arterial radius. The slope flattens with increasing pressure, because κ also increases.[34]

Being aware of this, it becomes clear that $s_{S,D}$ decreases with increasing *mean blood pressure*. It is therefore valuable for monitoring relative changes in blood pressure during stimulation, corresponding to ANS activity.

For the calculation of $s_{S,D}$ the previously detected minimum of a pulse was subtracted from its maximum.

3.3.2 Gauss Fitting

To obtain the forward and backward wave from a pulse wave, a Gauss fitting algorithm was implemented and tested for this thesis. The method is based on the assumption that a pulse wave is shaped like a Gaussian bell curve (GBC) and the recorded signal is a superposition of GBCs. The dicrotic notch which would strongly contradict this assumption is assumed to be not massively affecting the signal measured non-invasively at the toe in this study. The signals recorded at these sites usually look like the one depicted in Figure 16. To decompose the pulse waves, the PPG signal was cut at the sites of the previously detected minima to allow separate analysis of each pulse.

To decompose the pulse waves, a slightly modified peak fitting function from [35] was used. The function uses a least-squares fitting approach to fit peaks into a set of data points. It is a command line function and supports multiple peak shapes to fit into the signal, including the desired GBC fitting. To ensure proper performance with respect to our pulse wave decomposition approach, the function was validated.

For validation, arbitrary GBCs were computed using the classic formula for GBC in Eq. 2.3.

$$y = f(x|\mu,\sigma) = \frac{1}{\sigma\sqrt{2\pi}} e^{\frac{-(x-\mu)^2}{2\sigma^2}} \tag{2.3}$$

The GBCs were then superimposed as shown in Figure 20 and disassembled using the peak fitting algorithm.

Different sizes and positions of peaks were tested to ensure proper peak separation. The peak fitting function also includes an option for baseline correction (BC). The BC was absolutely vital for the analysis, since drifts in the baseline are an issue which had to be expected in the patient's PPG signals. The BC was therefore included in the testing as well.

The validated algorithm was then applied to single pulses from an actual PPG signal. Different options for analysis were tested. It was tried to fit two or more peaks into the pulse to account for more than one reflection, but in the end, the fitting of two peaks had the lowest error. The same is true for different BC models. Together with the linear correction, quadratic and cubic approaches were tested, but the linear BC lead to the most accurate disassembly of a pulse and was therefore used in the following analysis.

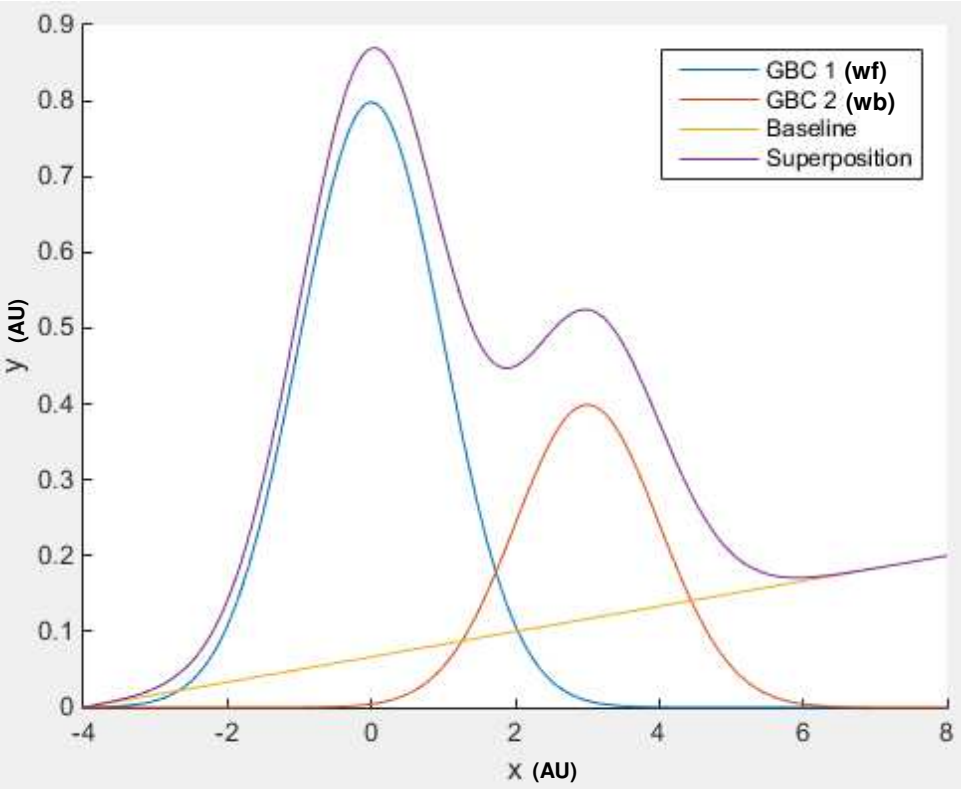

Figure 20: Sample pulse as used for validation of peak fitting algorithm.

According to the described method, each analyzed pulse yielded two GBCs, corresponding to wf (forward wave) and wb (backward wave). Returned parameters were *position*, *height*, *width* and *area* of the GBC, as well as a ready-made data plot.

3.3.3 Quality Control for Automated Signal Processing

Before and after analysis, the data was subjected to the following tests to ensure that it meets the required levels of quality.

Before analysis:

- **Peak match:** The number of previously detected min and max peaks was compared and each min peak was matched with a corresponding max peak. To be matched, a max peak needs to follow a min peak within a time window of 10 – 400 ms. Peaks which do not meet this criterion were considered irregular and were excluded from analysis.
- **PAT histogram**: Pulse arrival times of each pulse were calculated. Pulses where the PAT did not lie within 2 standard deviations were excluded from analysis. For visual control, a PAT histogram before and after peak removal was plotted. A typical result of PAT analysis is shown in Figure 21.

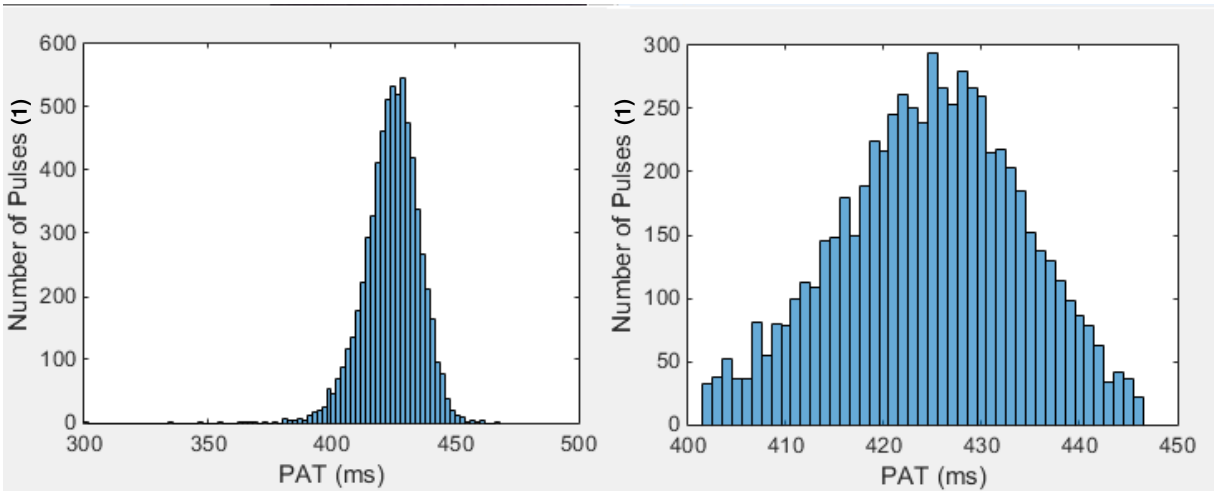

Figure 21: The PAT histogram of a typical measurement (healthy, with stimulation) before (left) and after clipping of all PATs with ±2 standard deviations.

After analysis:

The calculated Gauss parameters were checked for irregularities. Criteria for deletion of a pulse were:

- **Fitting Error of more than 5 %.**
- **Pulse length of more than 1600 ms.** This would indicate a section where PPG peaks have been removed before. The fitting algorithm however does not check for artefact windows and would simply interpret the gap between the remaining min peaks as one long pulse. Together with checking the error, the 1600 ms check eliminates the possibility of previously deleted artefacts to be taken into account for further analysis.
- **Amplitude of wb larger than amplitude of wf.**

3.3.4 Reflection Time

To monitor the change in perfusion, and thus in ANS activity, relative differences in the pulse wave velocity may be extracted. The Stiffness Index (SI), which is usually used to monitor vascular stiffness, works with the time difference ΔT between the maxima of wf and wb (Figure 22).

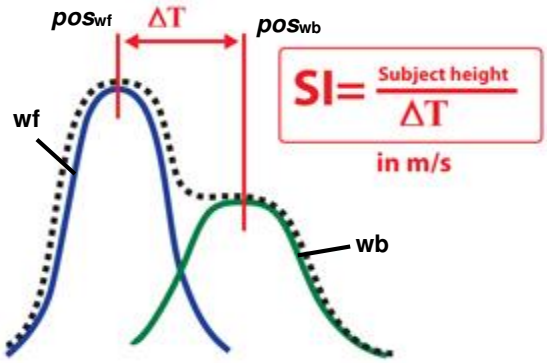

Figure 22: Scheme of the disassembled pulse wave. The time difference between wf and wb is an indicator for arterial stiffness. [36]

However, to monitor relative changes in ANS activity, a comparison of the reflection times ΔT between the pulses is sufficient. Lower ΔT means stiffer arteries, pointing to increased sympathetic activity. ΔT of each pulse was simply calculated as such given in Eq. 2.4:

$$\Delta T = pos_{\mathrm{wb}} - pos_{\mathrm{wf}} \tag{2.4}$$

3.3.5 Reflection Index

Vascular stiffness does not only influence the speed with which a pulse wave travels, but also the amount of energy that is lost along its path. Decreased arterial stiffness leads to higher damping of the pulse wave.

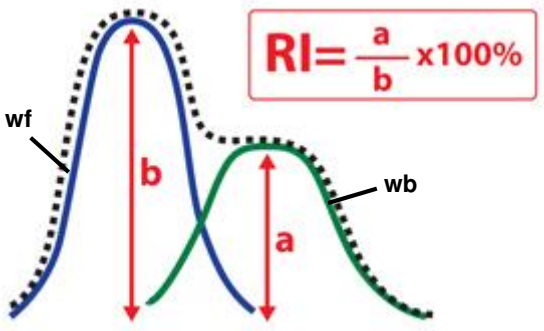

Figure 23: Scheme of the disassembled pulse wave. The relative amplitude of wb is an indicator for arterial stiffness. [36]

The reflection index RI (%) indicates the relative height of wb compared to wf and is calculated as shown in Figure 23. The height of both peaks was already available from the peak fitting algorithm and could easily be used in the formula.

Accordingly, both indices, RI and ΔT are expected to deliver redundant information about arterial stiffness which is influenced e.g. by aVNS.

4 Results

4.1 Validation of the Gauss Fitting Algorithm

Artificial Signals

The Gauss fitting algorithm was validated using artificial superimposed GBCs.

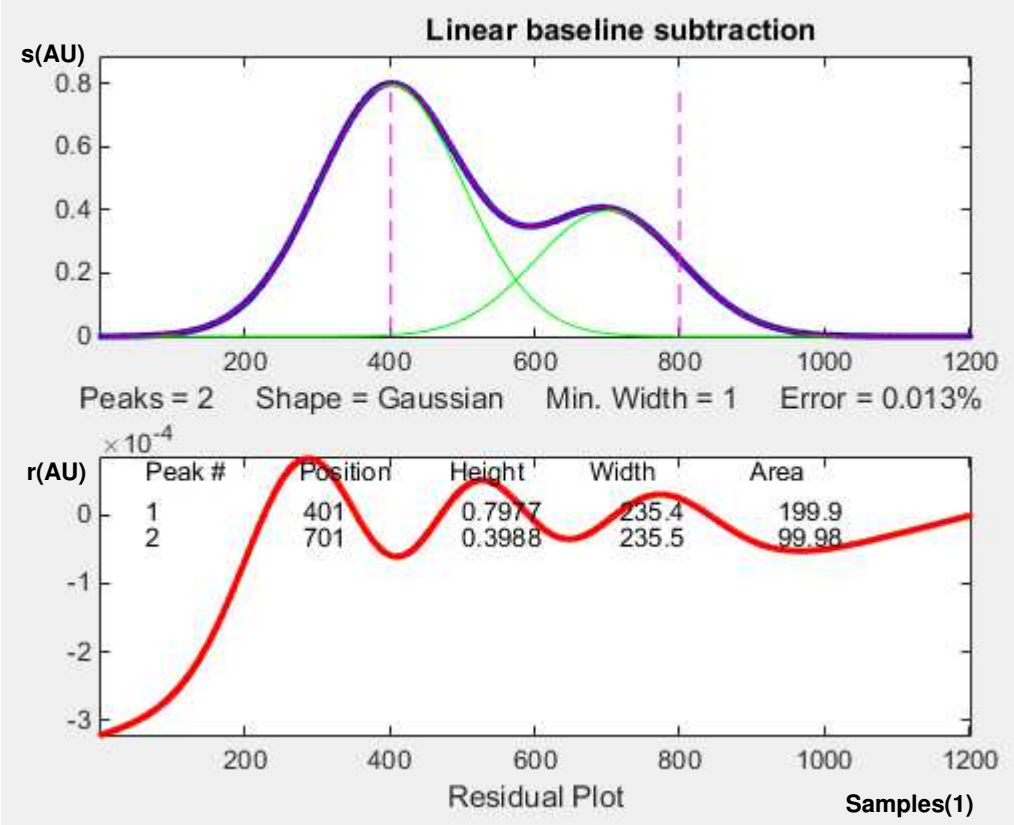

Figure 24: Gauss fitting of the generic signal from Figure 20. Blue: Input signal with the baseline already subtracted. Green: The fitted GBCs. Red: Residual plot. Error = 0.013 %.

For the baseline correction, linear, quadratic and functions of higher order were available. Linear (Figure 20 and Figure 24) and quadratic (Figure 25) options were tested, yielding errors of < 0.1 %.

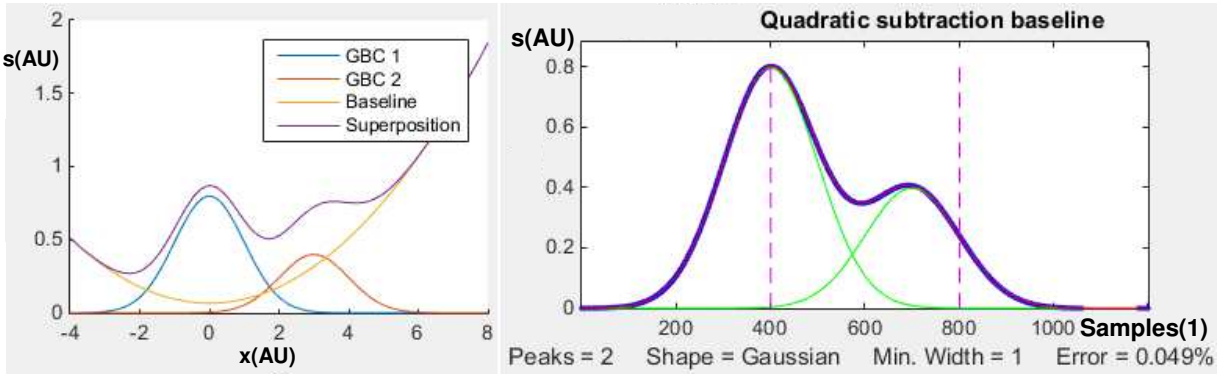

Figure 25: Test signal with quadratic baseline. The peaks were fitted with an error of 0.049 %.

Figure 26 shows further generic pulse waves and how they were decomposed by the Gauss fitting algorithm.

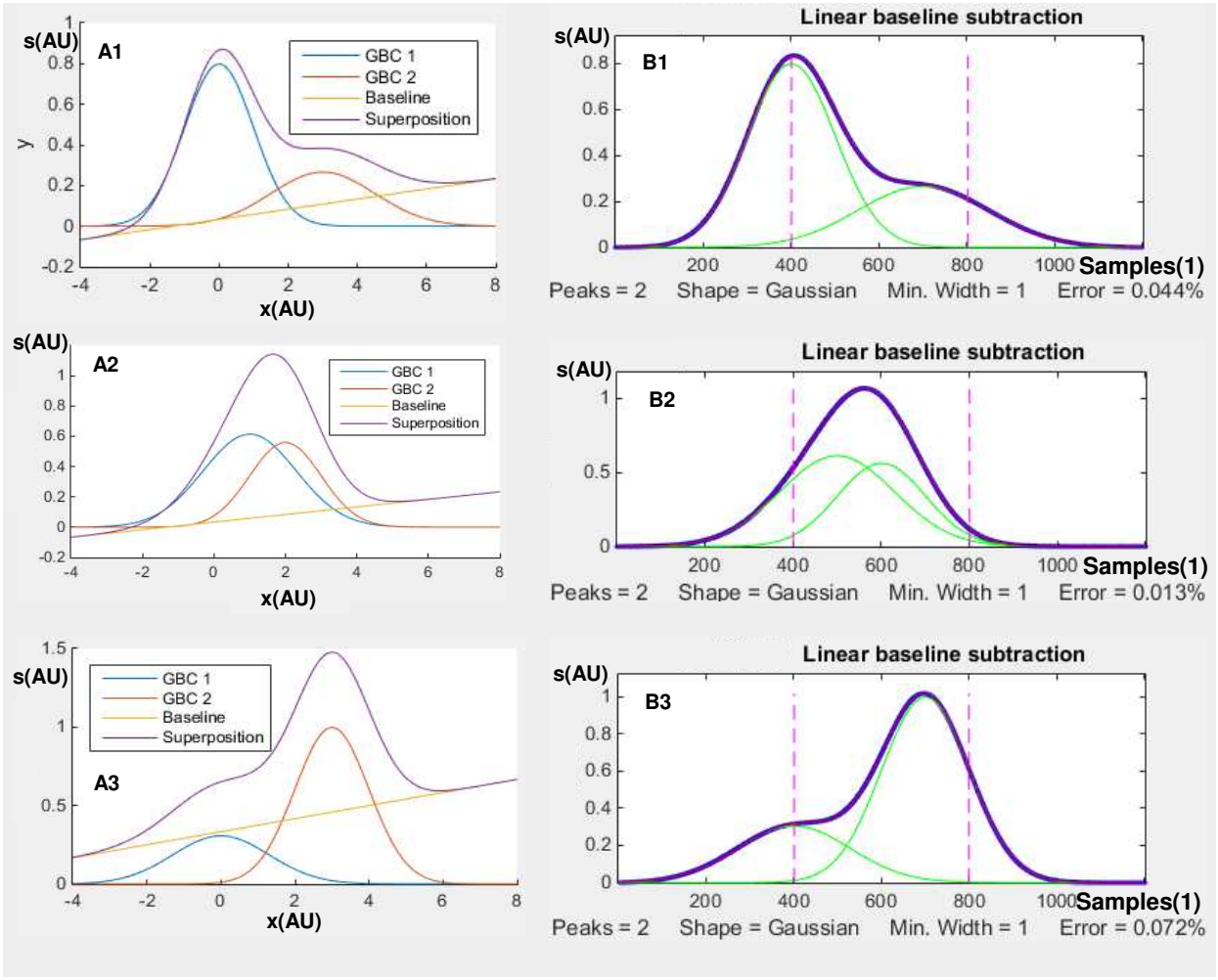

Figure 26: Examples of generic pulse waves (A1-A3) decomposed with the peak fitting algorithm (B1-B3).

Real Measured Signals

Preliminary tests had shown that, for actual PPG signals, linear baseline correction and the fitting of 2 peaks would yield the most promising results (smallest errors, Table 2). Therefore, the validation was performed with an emphasis on this parameter set.

	Fitting Error (%)
Linear Baseline, 2 Peaks	3,61 ± 0,62
Linear Baseline, 3 Peaks	4,89 ± 5,59
Quadratic Baseline, 2 Peaks	3,74 ± 1,23
Quadratic Baseline, 3 Peaks	7,54 ± 10,58

Table 2: Average fitting error from random pulse waves (N=50) analyzed with different parameters. The pulse waves were taken from real PPG signals.

Before Gauss fitting was performed, min and max peaks were matched (see 3.3.3). This control mechanism is crucial for further processing of the data. Usually, no more than 0.1 % of all peaks were removed by it. More pulses (5 – 10 %) were removed by histogram analysis. Only the pulses with PATs of no more than 2 standard deviations were left over for Gauss fitting.

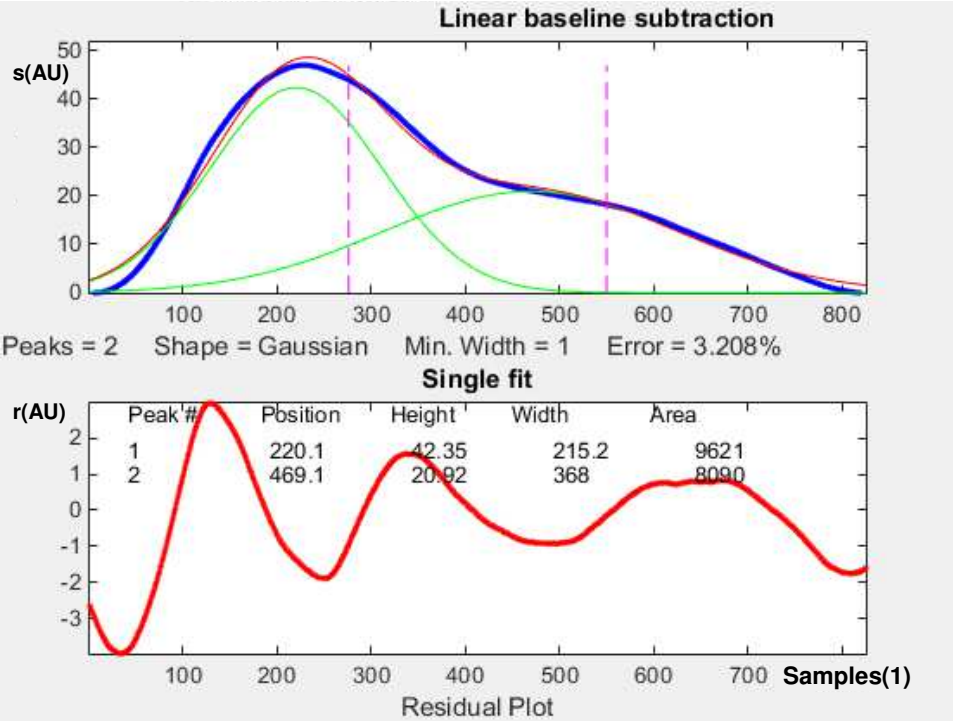

Figure 27: Visualization of the Gauss fitting process in a pulse wave as it was recorded during the study.

The decomposition of a single pulse is visualized in Figure 27. Correct fitting was highly dependent on signal quality which again, is dependent on the condition of the patient's vascular system, but also on the measurement itself.

The quality control mechanisms proved to be essential in the decomposition process and also showed that signal quality is crucial in terms of obtaining useful results. The last step of quality control usually removed another 5 – 10 % of all pulses. Altogether, in a regular signal, 10 – 20 % of all pulses were removed from the analysis. Other signals however were stripped of up to 80 % of their pulses by the quality control mechanisms, with the remaining data being very questionable.

The greatest difficulties arise when the incision between forward and backward wave is missing. This mostly occurred in diabetic patients with stiffer vessels and more advanced PVD. While the fitting itself works fine, the algorithm only aims to keep the fitting error as low as possible without regarding actual physical limitations. As shown in Figure 29, the form of the pulse wave causes the algorithm to assume the backward wave may have a higher amplitude than the forward wave. Since this is not possible, such results were dismissed by post processing quality control. Many measurements of diabetic patients showed this type of pulse waves and need to be considered useless. However, the same patients also delivered useful data in some sessions.

Figure 28 shows a boxplot of the fitting errors occurring during analysis of a PPG signal. The values match what was to be expected after validation of the algorithm and the results in Table 2.

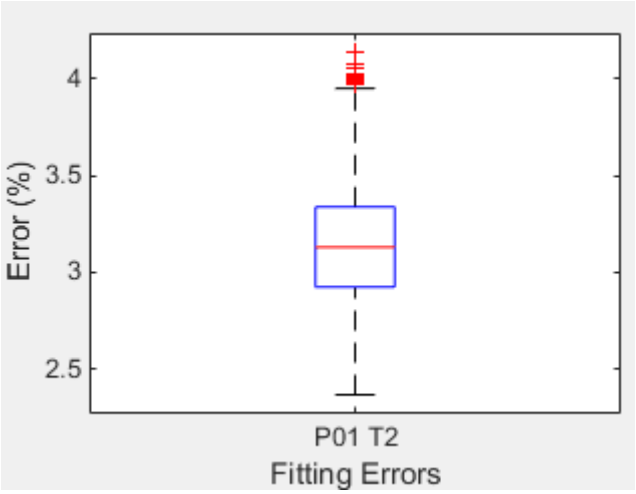

Figure 28: In a standard PPG signal, fitting errors are mostly lower than 4 %. Errors of >5 % can therefore be used for detection of artefact areas.

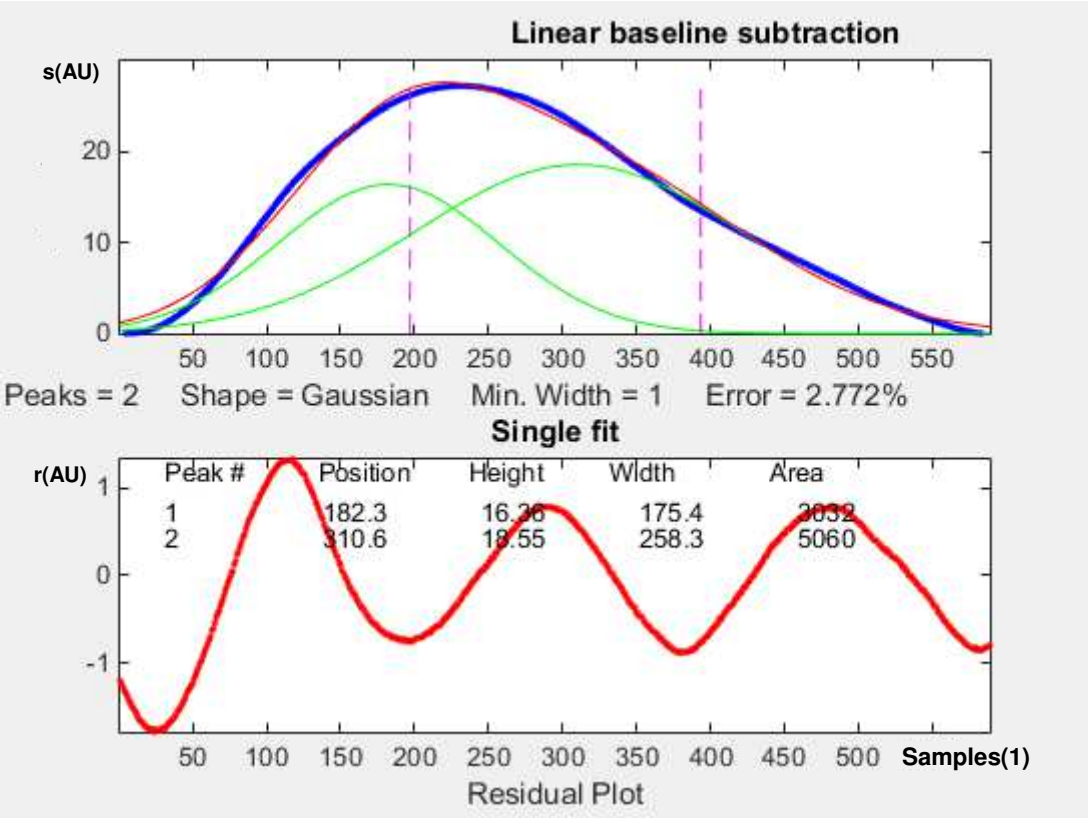

Figure 29: With a missing incision in the original pulse wave and the flat slope on the right side of the peak, the algorithm finds an ideal fit for two peaks that cannot represent the actual forward and backward waves.

Data Compression and Reconstruction

For successfully decomposed signals, different parameters are available which can be used for analysis like in 3.3.4 and 3.3.5. However, parametrization can of course help with compression of the data. The original PPG signals are sized around 22 MB. Furthermore, the data file of Gauss parameters, when including x – y plots of forward and backward waves, is around 70 MB in size. For this study alone, with a (theoretical) total of 80 – 100 datasets, this yields a total of ~10 GB data.

The fitting algorithm returns all necessary parameters for reconstruction of the pulses. By also conserving the starting time (these are actually the positions of the min peaks in the PPG signal) of each pulse, every pulse can be reconstructed with its correct length and placed in a vector consecutively.

Figure 30 shows that the x – y plots delivered by the fitting algorithm can be reconstructed exactly using the Gauss parameters and therefore don't need to actually be saved in the data file. Accordingly, Figure 31 shows a comparison of an original signal and one that was reconstructed from Gauss parameters, baseline data and starting times.

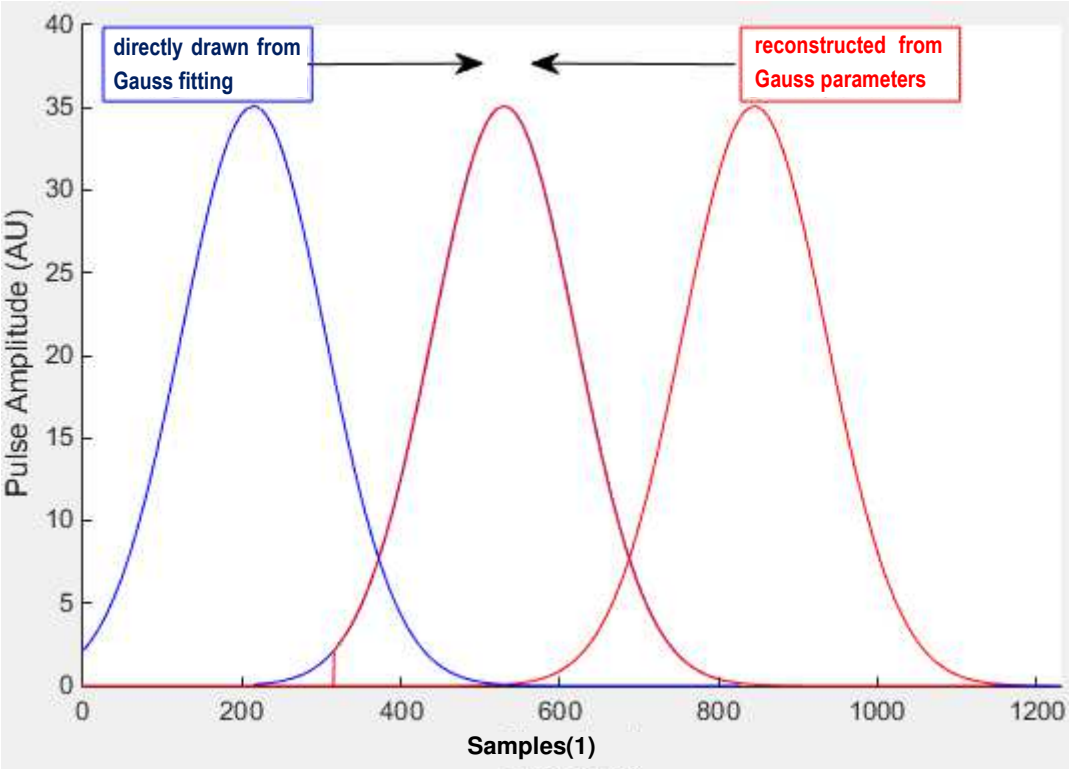

Figure 30: A foreward pulse wave. The blue pulse is a simple plotted set of data points as it is resturned by the Gauss fitting algorithm. The red pulse was calculated using parameters the analysis returned. When both pulses are overlayed (middle), they match each other exactly.

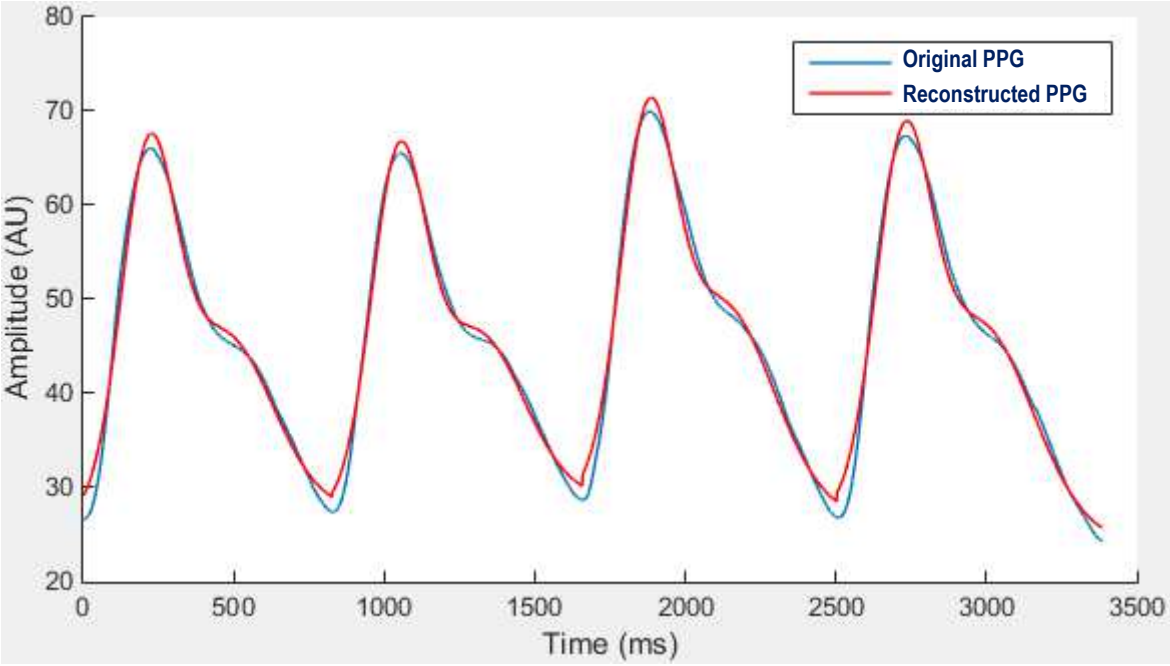

Figure 31: Comparison of an original and a reconstructed PPG signal.

Error values of such a reconstructed signal are in the range of 3 – 4 % over the whole signal. In return, the amount of data to be stored is reduced drastically. One set of Gauss parameters is about 500 KB, which is only about 2 % of the original size of a pulse signal. At the same time, it contains all the information of the decomposed pulse waves as well.

4.2 Application on Study Data

4.2.1 Systolic-Diastolic Volume Deflection

The systolic-diastolic volume deflection ($s_{S,D}$) in a PPG signal is an inverse indicator for the patients mean blood pressure. Figure 32 and Figure 33 show exemplary $s_{S,D}$ values of healthy patients with and without stimulation, to show the feasibility of application. In both cases, the values show high variability, but also a definite downward trend over the whole measurement. This indicates a rise in mean blood pressure and a possible increase in stress or sympathetic activity.

In contrast, $s_{S,D}$ of the sample diabetic patients do not show that much variability. However, the values of the diabetic patient slightly increase. The stimulated patient (Figure 34) shows a slightly different behavior compared to the diabetic without stimulation (Figure 35).

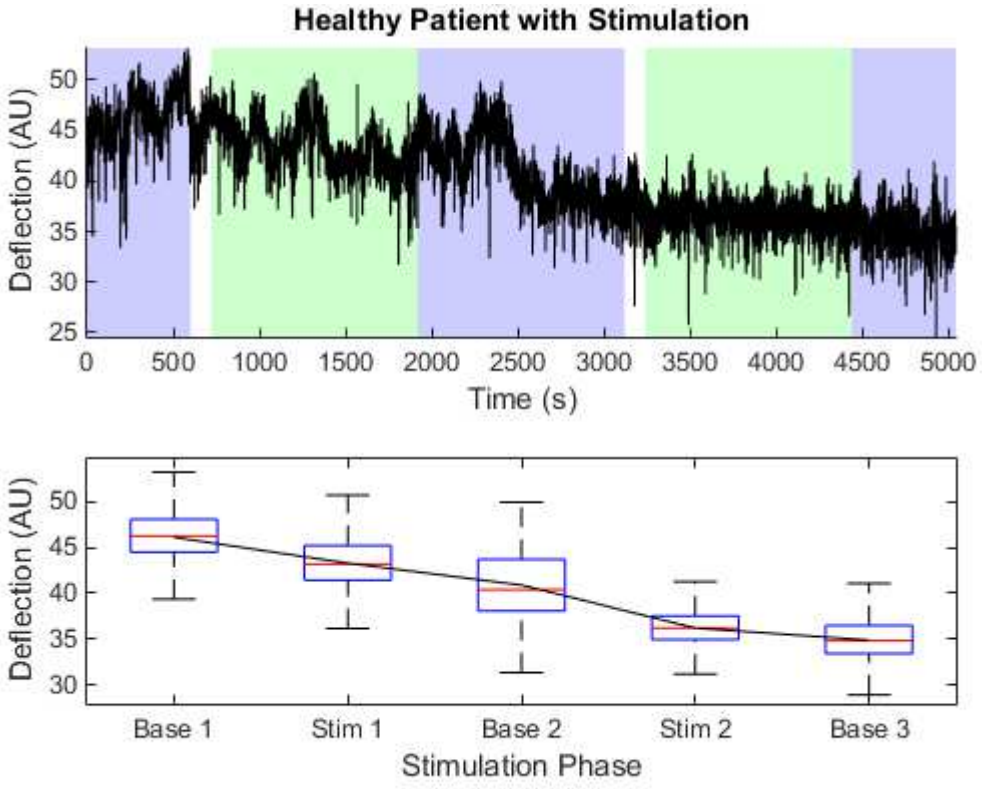

Figure 32: Systolic-diastolic volume deflection of a healthy patient during a measurement session with stimulation. The sections with colored background in the upper graph correspond to the stimulation sequence presented in Figure 11. The lower section shows boxplots for the different phases of stimulation of the above plot.

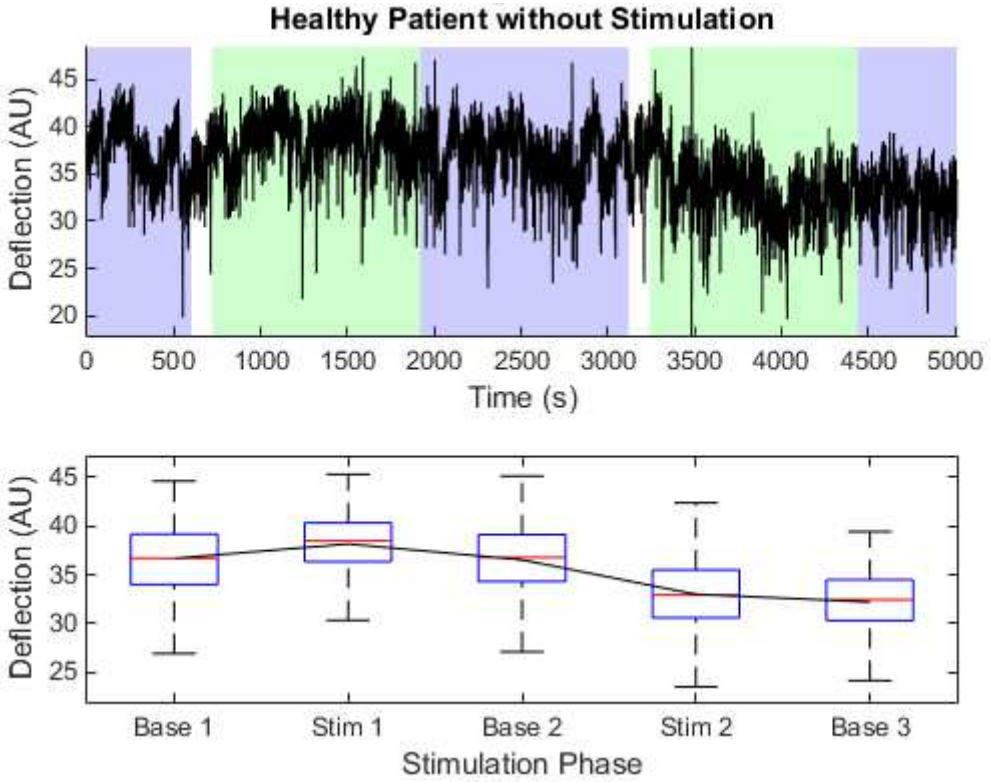

Figure 33: Systolic-diastolic volume deflection of a different healthy patient during a measurement session without stimulation. The sections with colored background in the upper graph correspond to the stimulation sequence presented in Figure 11. In this case, stimulation was never on. The lower section shows boxplots for the different phases of stimulation.

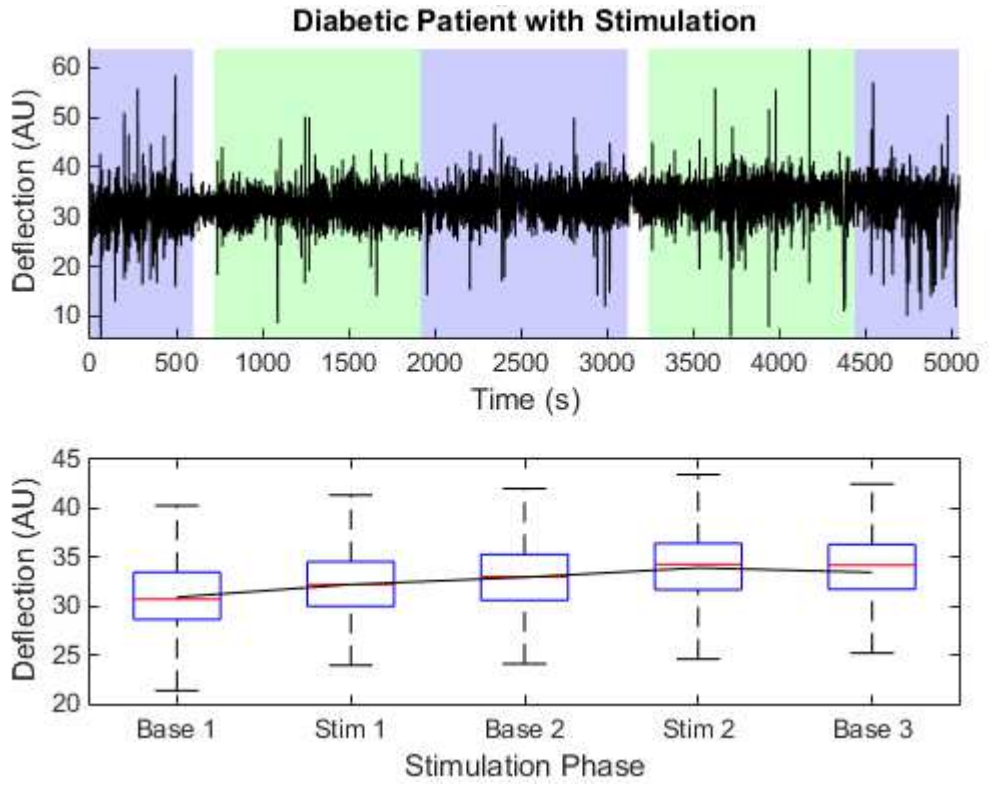

Figure 34: Systolic-diastolic deflection of a diabetic patient during a measurement session with stimulation. The sections with colored background in the upper graph correspond to the stimulation sequence presented in Figure 11. The lower section shows boxplots for the different phases of stimulation.

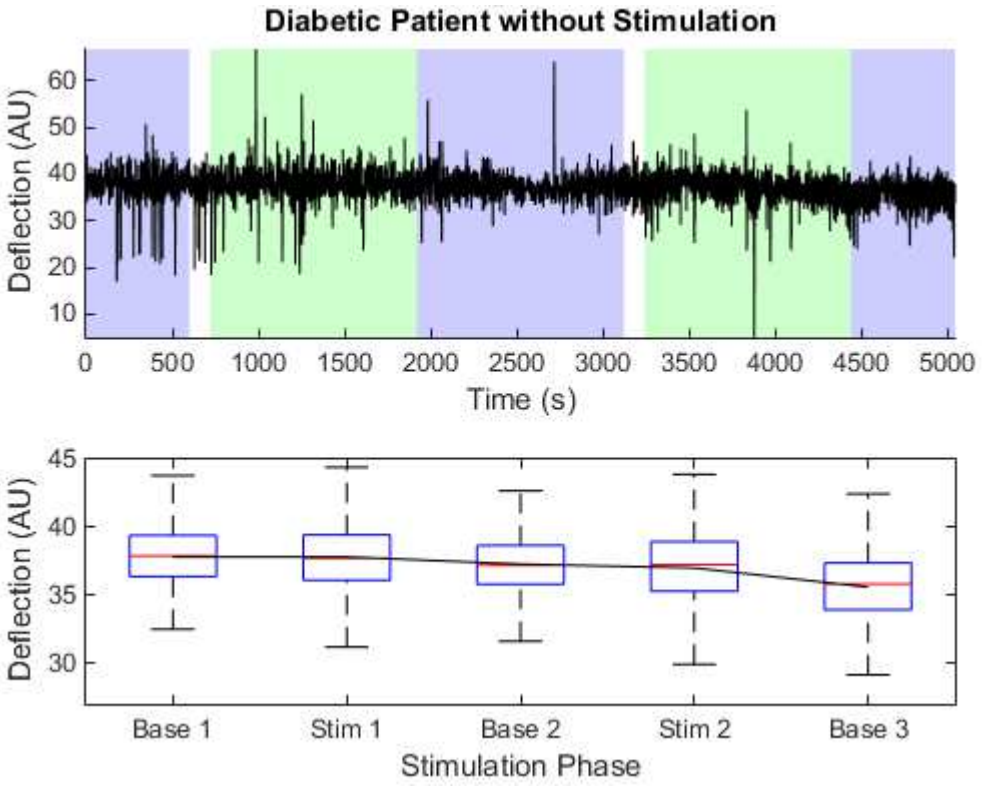

Figure 35: Systolic-diastolic volume deflection of a diabetic patient during a measurement session without stimulation. The sections with colored background in the upper graph correspond to the stimulation sequence presented in Figure 11. In this case, stimulation was never on. The lower section shows boxplots for the different phases of stimulation.

4.2.2 Reflection Time

Reflection times ΔT are a measure for arterial stiffness and can therefore be used as a relative indicator for ANS activity. Rising ΔT can be an indicator for reduced sympathetic activity. The data of the healthy patients (Figure 36 and Figure 37) shows some distinctive variability, but a real upward or downward trend cannot be seen over the whole measurement. The slow alterations in the ΔT values could be interpreted as regulatory processes. The diabetic patients (Figure 38 and Figure 39) again show quite stable values, ΔT varies more quickly. The variation seems more random, less directed and is therefore less likely to originate from a regulatory process. Still, even though they are somewhat occluded by the quick variation, slower and weaker, possibly regulatory processes can also be seen in the diabetic patients. Again, the datasets show no particular trends over the whole measurements.

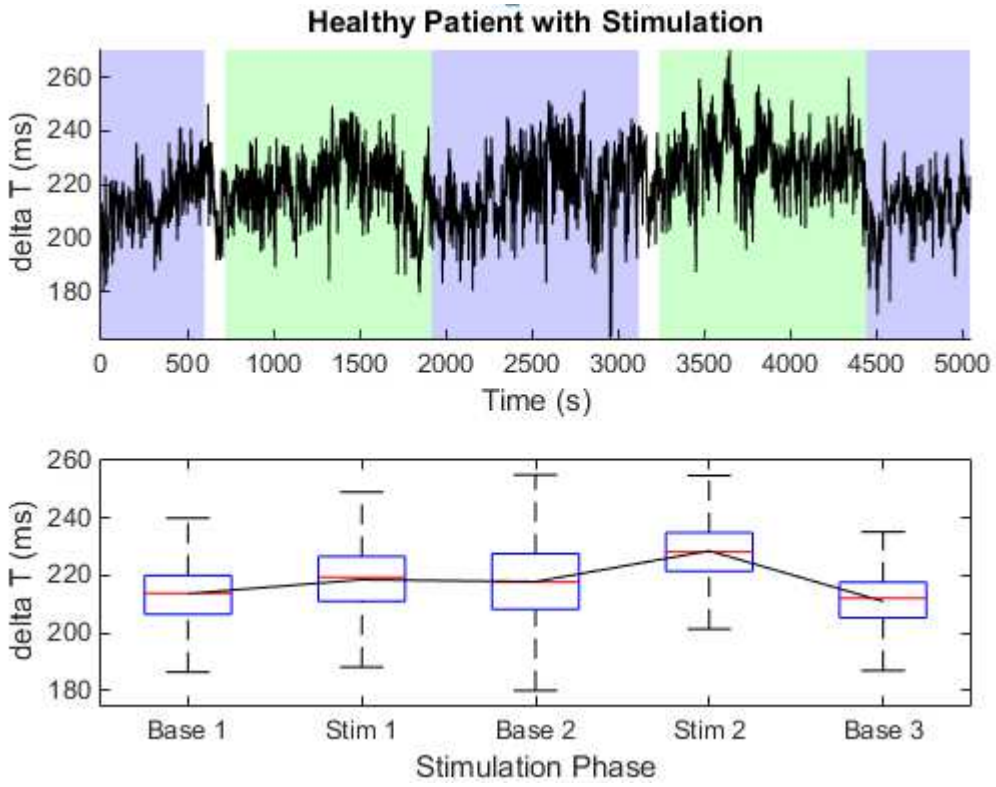

Figure 36: Reflection times of a healthy patient during a measurement session with stimulation. The sections with colored background in the upper graph correspond to the stimulation sequence presented in Figure 11. The lower section shows boxplots for the different phases of stimulation.

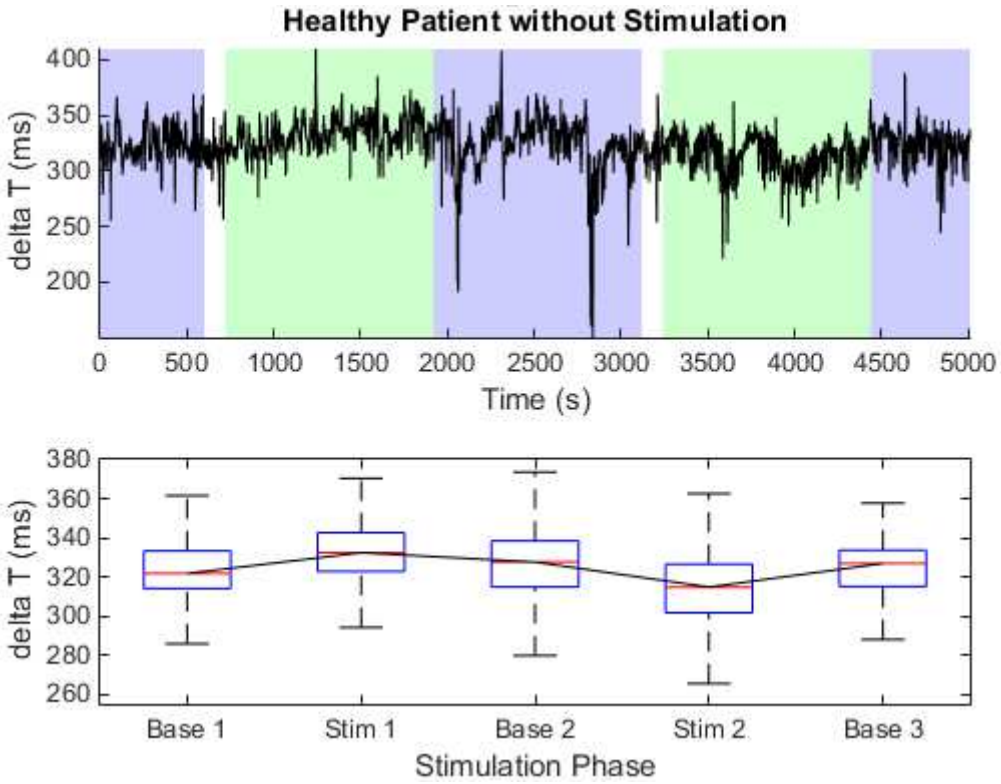

Figure 37: Reflection times of another healthy patient during a measurement session without stimulation. The sections with colored background in the upper graph correspond to the stimulation sequence presented in Figure 11, in this case however, stimulation was never on. The lower section shows boxplots for the different phases of stimulation.

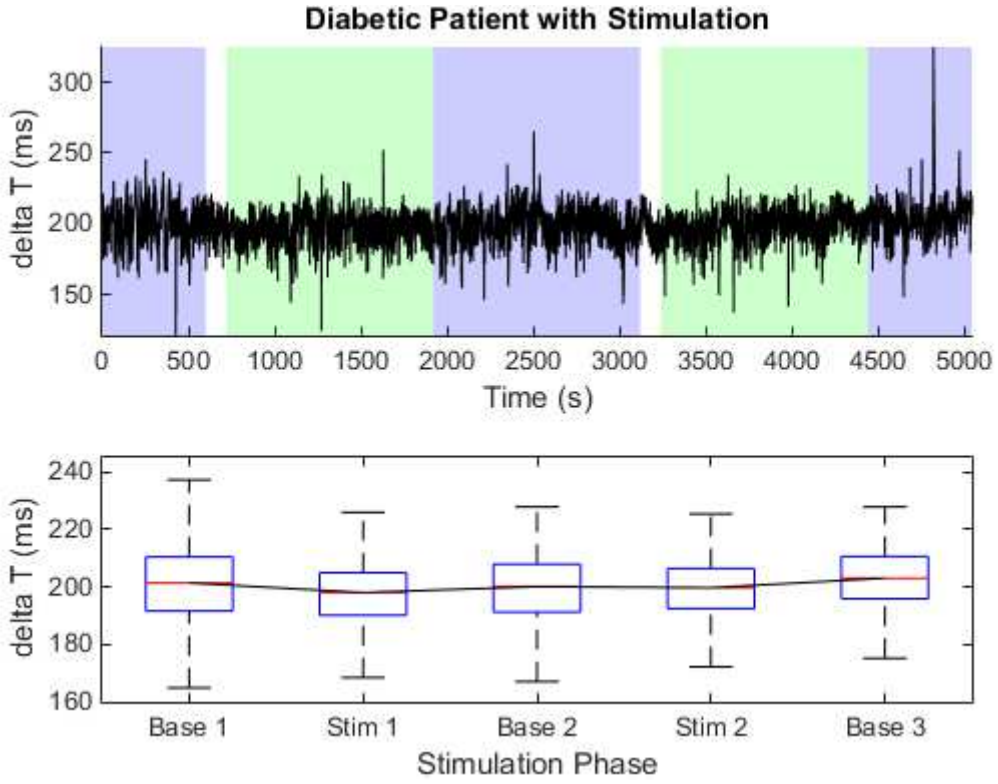

Figure 38: Reflection times of a diabetic patient during a measurement session with stimulation. The sections with colored background in the upper graph correspond to the stimulation sequence presented in Figure 11. The lower section shows boxplots for the different phases of stimulation.

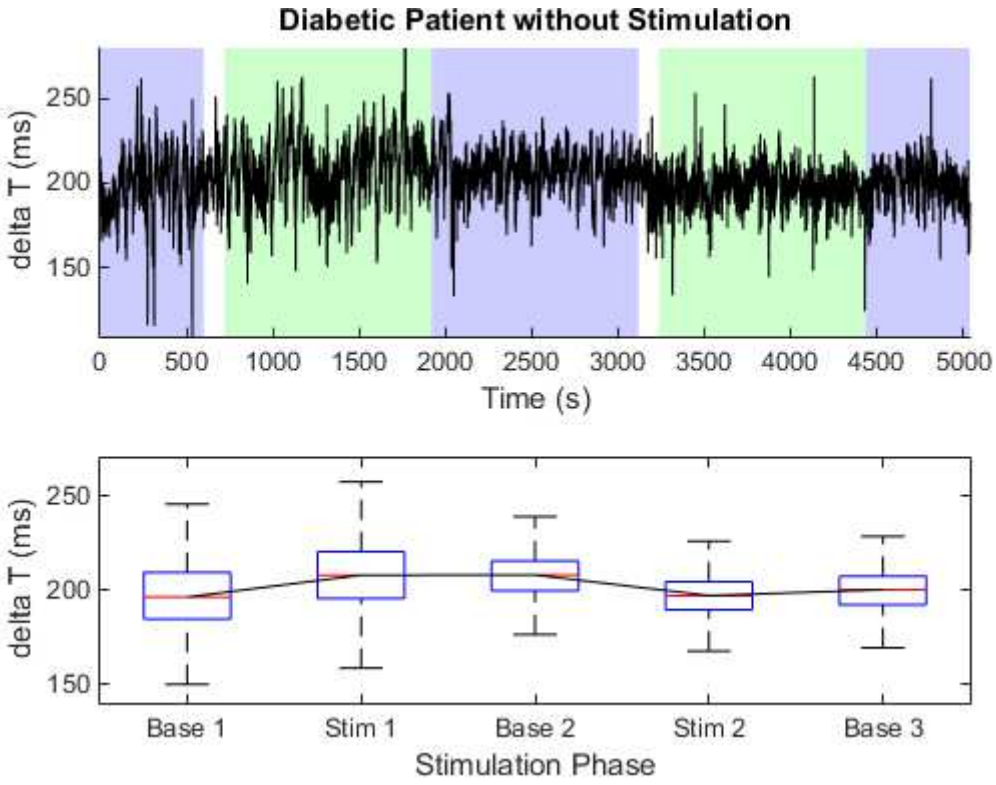

Figure 39: Reflection times of a diabetic patient during a measurement session without stimulation. The sections with colored background in the upper graph correspond to the stimulation sequence presented in Figure 11, in this case however, stimulation was never on. The lower section shows boxplots for the different phases of stimulation.

4.2.3 Reflection Index

The reflection index (RI) is a measure for the amplitude ratio of wb compared to wf. A higher RI means wb was subjected to less damping, indicating stiffer walls, and thus maybe increased sympathetic activity.

The sample RIs of the healthy patients (Figure 40 and Figure 41) show a more distinctive, slower variability than the RIs of the diabetic patients (Figure 42 and Figure 43). The RIs of diabetics vary more quickly, but with less amplitude than the RIs of healthy patients. However, in this case, the diabetics show a definite trend of rising RI over the measurement, while healthy patients show no such specific tendencies.

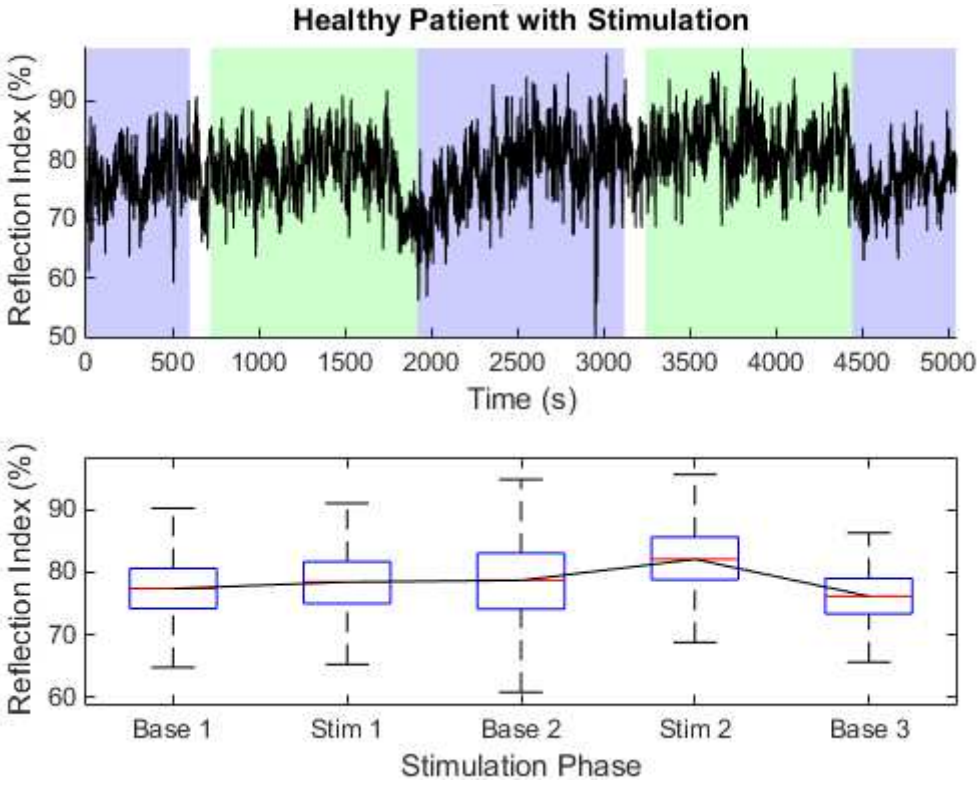

Figure 40: Reflection index of a healthy patient during a measurement session with stimulation. The sections of the colored background of the upper graph correspond the stimulation sequence presented in Figure 11. The lower section shows boxplots for the different phases of stimulation.

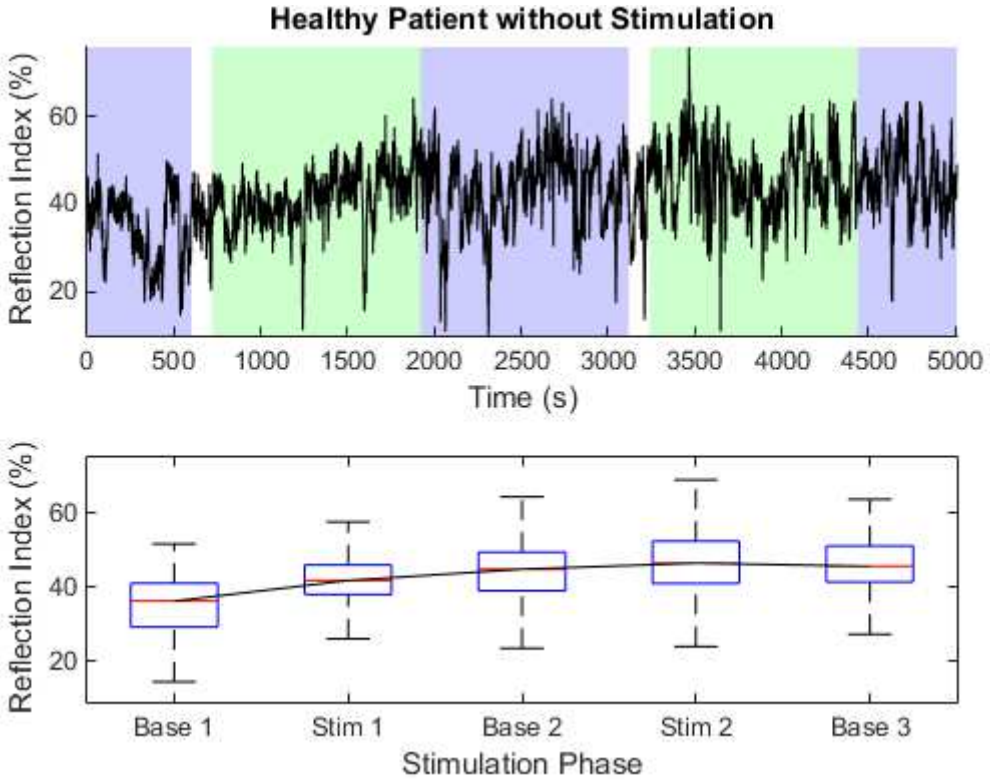

Figure 41: Reflection index of a healthy patient during a measurement session without stimulation. The sections of the colored background of the upper graph correspond the stimulation sequence presented in Figure 11, in this case however, stimulation was never on. The lower section shows boxplots for the different phases of stimulation.

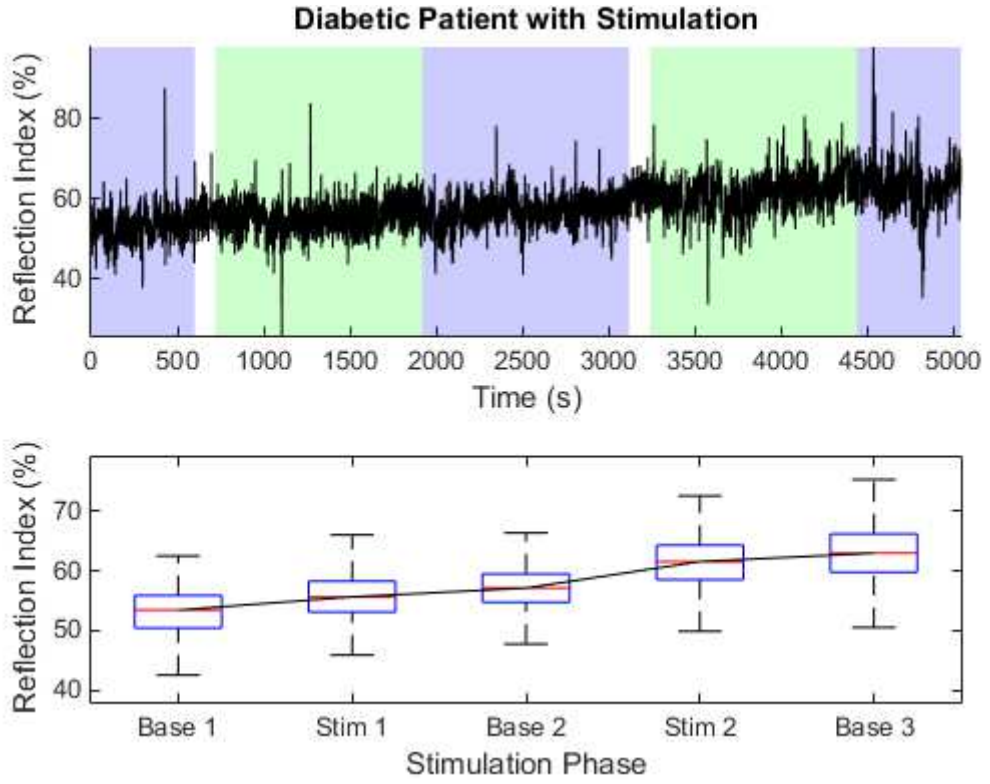

Figure 42: Reflection index of a diabetic patient during a measurement session with stimulation. The sections of the colored background of the upper graph correspond the stimulation sequence presented in Figure 11. The lower section shows boxplots for the different phases of stimulation.

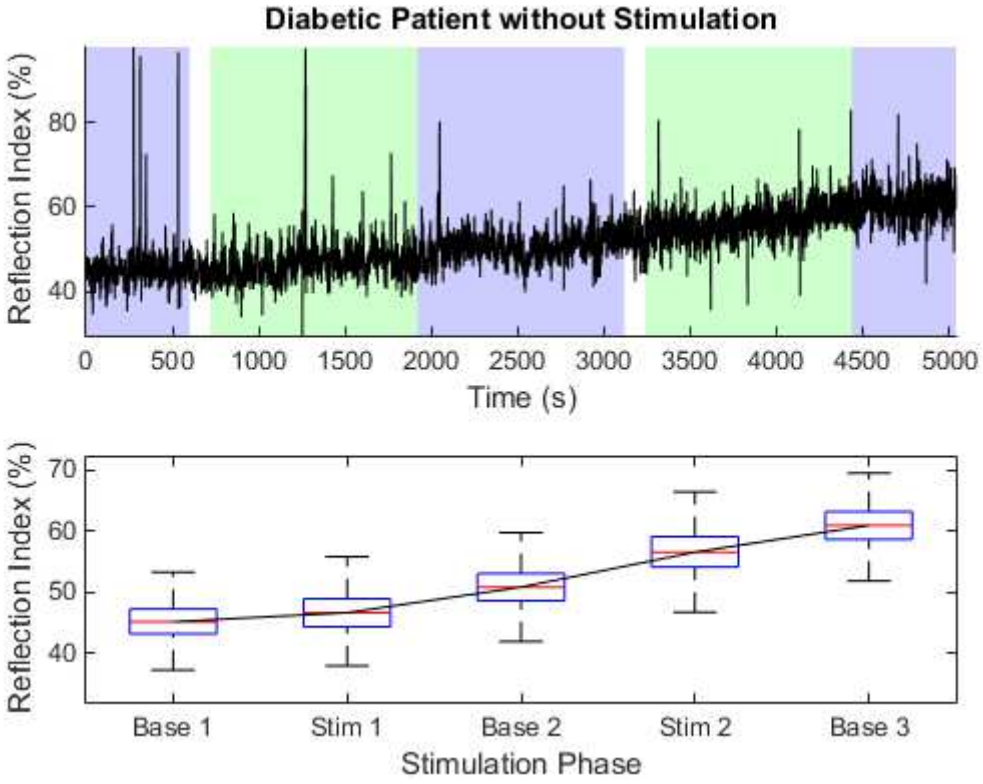

Figure 43: Reflection index of a diabetic patient during a measurement session without stimulation. The sections of the colored background of the upper graph correspond the stimulation sequence presented in Figure 11, in this case however, stimulation was never on. The lower section shows boxplots for the different phases of stimulation.

5 Discussion

This thesis reviews and evaluates a small number of methods for pulse wave analysis. In particular, PPG signals from healthy and diabetic patients had to be decomposed into forward and backward waves. Methods for computing reflection times and reflection indices, as markers for arterial stiffness and ANS activity, were assessed.

A pulse wave, as it is created by the human heart, may be estimated by the form of a Gaussian distribution. It is superimposed with its several reflections and can be recorded as a typical PPG pulse. The crucial point in successfully using the desired parameters was to find an effective method for pulse wave decomposition, since they require knowledge about forward and reflected waves. In another project, empirical mode decomposition was tested as a method to decompose a pulse signal. However, this approach could not yield any satisfying results. In [37], independent component analysis (ICA) was used to extract forward and backward components from a PPG signal. The pulse wave was decomposed and the existence of several reflections could be shown. However, just like the Multi-Gaussian approaches in [31] and [32], the ICA method does not yield the incident and reflected wave of a pulse wave. For direct extraction of parameters like RI and SI, another, more practicable approach needed to be developed. For this method, similar to [33], a Gaussian nature of the particular pulses was assumed and exploited in order to extract the forward and backward waves from the PPG.

Min/Max Peak Detection

For the fitting of single Gaussian peaks into the signal, a controlled environment has to be created. Hence, the PPG signal was split into single pulses. The utilized ECG detection algorithm has been developed and verified in a preceding thesis [29]. The obtained ECG peaks were used to detect minima and maxima in the PPG signal following the respective heartbeat. Defined windows were used, to check for maximum or minimum values within them. These windows were delicate to adapt to the signal at hand. Distance of the measuring site from the heart and the expected PAT had to be taken into account. For the detection in finger and toe signals, different sets of windows were used. Although the resulting detection algorithms worked fine, an ideal “one-fits-all” window setting could not be found, since even at the same measuring site, PAT differences between patients were large. However, larger windows could not have been used due to a then increasing number of wrongly detected peaks. To ensure proper detection for the following analysis, the results were always checked and corrected manually.

To further automate PPG detection, adaptive windows, based on a quick analysis of the input signal could help to reduce errors. The results would still need to be checked manually, but having better detection or more sophisticated post processing could greatly reduce the time needed for this final manual control.

Gauss Peak Fitting

The PPG signal could now be snipped into single pulses to fit Gauss peaks into. The Gauss fitting algorithm was developed at the University of Maryland. It was slightly modified and validated for the use with our PPG signals. The algorithm uses an iterative least-squares approach to fit 2 Gauss peaks into a signal.

Validation yielded very promising results. Arbitrarily computed superpositions of Gauss peaks were decomposed yielding errors of < 0.1 %. The fact that there are any errors at all is due to the formula used in the fitting algorithm for computing a Gauss pulse. It is different from the standard formula in Eq. 2.3, which is due to faster computation times. Nevertheless, the algorithm was tested against peaks which were computed using the standard formula in Eq. 2.3 and performed very well.

When applied to a real PPG signal, the algorithm directly generates parameters which contain the Gauss peaks as well as the parameters necessary to compute them. These parameters could also directly be used to compute reflection time and reflection index. By applying pre- and post-processing tools it was possible to exclude results that didn't make any sense while easily creating conclusive figures to outline the patient's performance during measurements. The fitting errors for the pulses were constantly below 5 %, making the 5 % threshold also eligible as an exclusion criterion during post-processing.

In the course of the study, the amount of data on the server and to transfer between one another constantly grew. When only the Gauss parameters are stored, the whole PPG signal can be reconstituted from them. A PPG signal of about 22 MB can be compressed to ~500 KB, a reduction of more than 97 %. Future applications on mobile devices might profit from such compressions. The reconstitution of course includes the error that occurred during Gauss analysis. With < 5 %, the accuracy might however be sufficient for many applications.

Although the fitting algorithm performed very well in general, several challenges still need to be addressed for studies like this. Many of the patients, especially the diabetic ones, yielded very poor quality data, up to the point that it could not be used for analysis at all. Reasons for this can be found in the general data acquisition methods as well as in the conducted analysis.

For data acquisition, a Nellcor™ pulse oximeter (Toe), and a BIOPAC® PPG sensor were used. The BIOPAC® sensor delivered unfiltered and completely unmodulated data. This however also led to undetectably small amplitudes during phases of vasoconstriction. Altogether, many finger signals were fragmented or contained so many artefacts that they were not considered at all in this thesis. The toe signals, recorded using the Nellcor™ device, which were analyzed here, were possibly filtered and modulated heavily by the device itself. The precise parameters of this filter could neither be assessed nor changed. The resulting signal was sometimes good to use, but in other cases, filtering probably led to the loss of important information. Especially when, in patients with stiffer vessels, the reflected wave started to wander towards the incident wave, remaining incisions in the signal might have been filtered away, leaving the fitting algorithm with no good point to start from. The resulting peaks were then often set at seemingly random positions, since the algorithm only uses the least error as a criterion for its fitting approach. More sophisticated methods for PPG recording, which are adapted to the physiological state, could help to improve the data quality immensely.

There is also still a lot of potential for optimization in the fitting algorithm itself. Setting up constraints for the Gauss peaks might lead to more realistic physiologic results in many cases, even though fitting errors would rise. For example, the two peaks can be set to having the same width. This would physiologically and physically make sense, since the width of the reflected wave should not change as long as there are no non-linear effects involved. First trials have actually shown promising results, producing a lot more realistic ratios for the peak amplitudes. This new approach also strongly improved the positioning of the peaks in the signal. The problems which arose from the possibly filtered PPG signal, as described in the previous paragraph, can be addressed with this method. A comparison of the two methods can be seen in Figure 44.

The new method also makes the algorithm more robust towards lower quality signals. A dataset in which 2.733 analyzed pulses (almost 50%) failed quality control before could then be analyzed with only 198 pulses (about 3%) failing quality control.

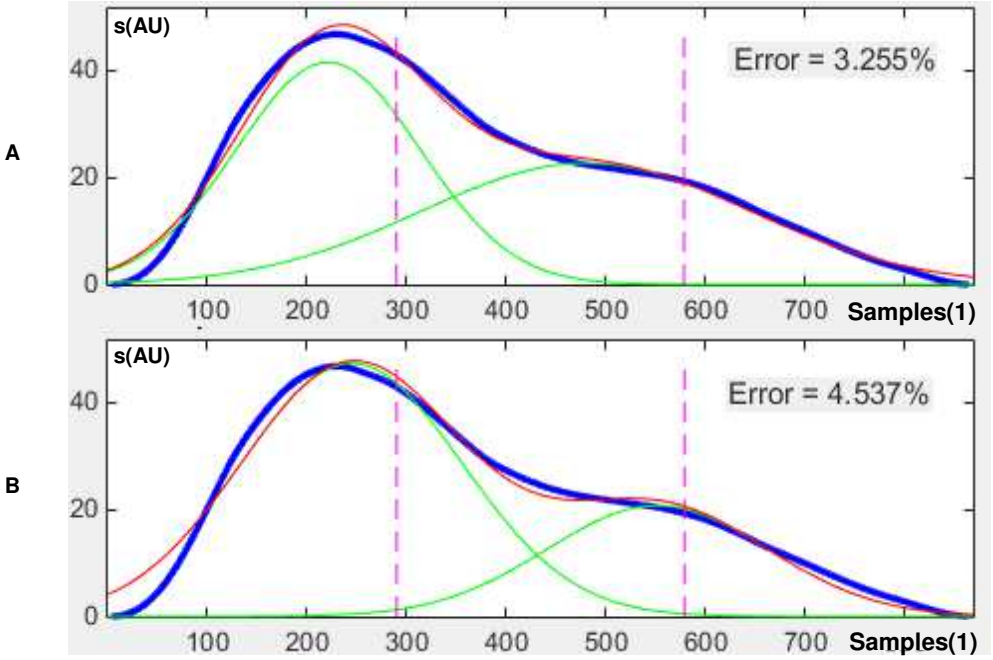

Figure 44: The same pulse is decomposed with unconstrained Gaussians (A) and fixed-width Gaussians (B). Even though the fitting error in (B) is larger, the fitted pulses seem to match their expected forms better than in (A).

Monitoring Parameters

The results from 4.2.1, 4.2.2 and 4.2.3 show consistent, but partially unexpected results. The general deficiency in the diabetic nervous system may clearly be seen in the graphs of Figure 34 or Figure 38. Regulatory deflections are hardly visible. This is true for most measurements of diabetic patients. Still, shown here are only single measurements. The described trends could be a coincidence. Valid statistics were not performed, but further investigation might be of use here. The sampled diabetic patients seem to show a steady rise in reflection index values, while reflection time and systolic-diastolic deflection show no such tendencies. This behavior points to increasing stiffness of the small arteries, without the larger arteries being affected. [38]

The results are consistently similar for patients with or without stimulation. For the investigated indices and patients, stimulation does not seem to cause any immediately visible effects during stimulation. Long term effects were not assessed. The same is true for healthy patients. Their values show slower, more distinct variability, they do not seem to be immediately influenced by stimulation. The only case where the stimulated diabetic shows a different behavior than the non-stimulated one is systolic-diastolic deflection. Here the rise in the stimulated patient's $s_{S,D}$ points to decreased sympathetic activity, which is an expected effect of aVNS.

In case of the healthy subjects however, a constant drop in systolic-diastolic deflection points to increasing mean blood pressure over time.

Whenever indices showed a trend over the measurement, they were mainly pointing towards sympathetic, not parasympathetic effects. However, these trends also happened without any stimulation, so they are most likely not caused by the stimulation. Other factors, like the new environment and treatment probably influence the patient's reaction. Further analysis are necessary, including long-term evaluations of stimulation effects.

Conclusion and Outlook

The decomposition of a PPG signal into Gauss peaks certainly houses a lot of potential for quick, automated and sound analysis to be used for monitoring or even diagnostics.

The software so far is in a state, where it can analyze a set of patient data with one click, when PPG and min/max peaks are supplied. Further optimization can lead to even better results. Especially the future use of fixed width Gauss peaks will probably improve the program. Still, the availability of good quality signals is key to ensure constant useful results. Other signal acquisition techniques using good quality sensors without extensive and non-reproducible filtering should be used in the future to provide quality data.

Long-term application of stimulation might be of interest to monitor the development of the ANS over a longer period of therapy.

Further works, established on the grounds of the aVNS study will examine different aspects of it. While this work is a fairly technical one, concentrating on a good method for processing the PPG data, others will analyze blood pressure, respiration, O_2 saturation and many more concerning the effects of aVNS.

6 Abbreviations

AGE	Advanced glycation end product
ANS	Autonomous nervous system
AP	Action potential
ATP	Adenosine triphosphate
AV	Atrioventricular
aVNS	Auricular vagus nerve stimulation
BC	Baseline correction
BPI	Blood perfusion index
CNS	Central nervous system
DFI	Diabetic foot infection
DFU	Diabetic foot ulcer
DM	Diabetes mellitus
DVP	Digital volume pulse
ECG	Electrocardiogram
ES	Electrostimulation
GBC	Gaussian bell curve
GUI	Graphical user interface
HR	Heart rate
HRV	Heart rate variability
ICA	Independent component analysis
NS	Nervous system
PAD	Peripheral artery disease
PPG	Pulse plethysmography
PVD	Peripheral vascular disease
RI	Reflection index
RT	Reflection time
SDD	Systolic-diastolic volume deflection
SDDVP	Second derivative of digital volume pulse
SI	Stiffness index
VN	Vagus nerve
VNS	Vagus nerve stimulation

7 Bibliography

[1] “Diabetes: facts and figures,” *International Diabetes Federation*. [Online]. Available: http://www.idf.org/worlddiabetesday/toolkit/gp/facts-figures. [Accessed: 18-Mar-2015].
[2] L. Xu, K. Kanasaki, M. Kitada, and D. Koya, “Diabetic angiopathy and angiogenic defects,” *Fibrogenesis Tissue Repair*, vol. 5, p. 13, Aug. 2012.
[3] S. C. Wu, V. R. Driver, J. S. Wrobel, and D. G. Armstrong, “Foot ulcers in the diabetic patient, prevention and treatment,” *Vasc. Health Risk Manag.*, vol. 3, no. 1, pp. 65–76, 2007.
[4] J. Mendes, “Diabetic Foot Infections: Current Diagnosis and Treatment « Journal of Diabetic Foot Complications.” .
[5] J. C. S. Eugenijus Kaniusas, “Adaptive Auricular Electrical Stimulation Controlled by Vital BIOSIGNALS - Transition from Fixed to Adaptive and Synchronized Electrical Stimulation Controlled by Heart Rate Variability and Blood Perfusion.,” pp. 304–309, 2009.
[6] R. F. Schmidt, F. Lang, and M. Heckmann, *Physiologie Des Menschen: Mit Pathophysiologie*. Springer Berlin Heidelberg, 2007.
[7] “Action Potentials.” [Online]. Available: http://hyperphysics.phy-astr.gsu.edu/hbase/biology/actpot.html. [Accessed: 31-Aug-2015].
[8] “Chapter 11: Fundamentals of the Nervous System and Nervous Tissue.” [Online]. Available: http://classes.midlandstech.edu/carterp/Courses/bio210/chap11/lecture1.html. [Accessed: 29-Jul-2015].
[9] E. Kaniusas, *Biomedical Signals and Sensors I*. Berlin, Heidelberg: Springer Berlin Heidelberg, 2012.
[10] “Vagus Nerve-Mediated Immunity - Laboratory for Injury Research | UC San Diego School of Medicine,” *UC San Diego Health Sciences*. [Online]. Available: http://surgery.ucsd.edu/divisions/trauma-burn/research/eliceirilab/vagal-nerve/Pages/default.aspx. [Accessed: 01-Aug-2015].
[11] E. P. Van Der Zanden, G. E. Boeckxstaens, and W. J. de Jonge, “The vagus nerve as a modulator of intestinal inflammation,” *Neurogastroenterol. Motil. Off. J. Eur. Gastrointest. Motil. Soc.*, vol. 21, no. 1, pp. 6–17, Jan. 2009.
[12] L. Steinman, “Elaborate interactions between the immune and nervous systems,” *Nat. Immunol.*, vol. 5, no. 6, pp. 575–581, Jun. 2004.
[13] G. Matteoli and G. E. Boeckxstaens, “The vagal innervation of the gut and immune homeostasis,” *Gut*, vol. 62, no. 8, pp. 1214–1222, Aug. 2013.
[14] “Long QT Syndrome Knowledge Base: Electrical Activity of the Heart.” [Online]. Available: http://www.research.chop.edu/programs/lqts/heartfam.php. [Accessed: 05-May-2015].
[15] “Diagnosis and Classification of Diabetes Mellitus,” *Diabetes Care*, vol. 33, no. Suppl 1, pp. S62–S69, Jan. 2010.
[16] D. LeRoith, S. I. Taylor, and J. M. Olefsky, *Diabetes Mellitus: A Fundamental and Clinical Text*. Lippincott Williams & Wilkins, 2004.
[17] S. Melmed, *Williams Textbook of Endocrinology*. Elsevier/Saunders, 2011.
[18] N. Ahmed, “Advanced glycation endproducts—role in pathology of diabetic complications,” *Diabetes Res. Clin. Pract.*, vol. 67, no. 1, pp. 3–21, Jan. 2005.
[19] N. R. Barshes, M. Sigireddi, J. S. Wrobel, A. Mahankali, J. M. Robbins, P. Kougias, and D. G. Armstrong, “The system of care for the diabetic foot:

objectives, outcomes, and opportunities," *Diabet. Foot Ankle*, vol. 4, no. 0, Oct. 2013.
[20] L. L. Baker, R. Chambers, S. K. DeMuth, and F. Villar, "Effects of electrical stimulation on wound healing in patients with diabetic ulcers," *Diabetes Care*, vol. 20, no. 3, pp. 405–412, Mar. 1997.
[21] E. J. Peters, L. A. Lavery, D. G. Armstrong, and J. G. Fleischli, "Electric stimulation as an adjunct to heal diabetic foot ulcers: A randomized clinical trial," *Arch. Phys. Med. Rehabil.*, vol. 82, no. 6, pp. 721–725, Jun. 2001.
[22] T. Forst, A. Pfützner, R. Bauersachs, M. Arin, B. Bach, H. Biehlmaier, E. Küstner, and J. Beyer, "Comparison of the microvascular response to transcutaneous electrical nerve stimulation and postocclusive ischemia in the diabetic foot," *J. Diabetes Complications*, vol. 11, no. 5, pp. 291–297, Oct. 1997.
[23] S. Kampusch, E. Kaniusas, J. C. Széles. "Modulation of Muscle Tone and Sympathovagal Balance in Cervical Dystonia using Percutaneous Stimulation of the Auricular Vagus Nerve." in press, 2015.
[24] T. Yamamoto, "Vagus Nerve Stimulation Therapy: Indications, Programing, and Outcomes," *Neurol. Med. Chir. (Tokyo)*, no. 55, pp. 407–415, Apr. 2015.
[25] U. Albert, G. Maina, A. Aguglia, A. Vitalucci, F. Bogetto, C. Fronda, A. Ducati, and M. Lanotte, "Vagus nerve stimulation for treatment-resistant mood disorders: a long-term naturalistic study," *BMC Psychiatry*, vol. 15, p. 64, 2015.
[26] S. M. Sator-Katzenschlager, J. C. Szeles, G. Scharbert, A. Michalek-Sauberer, A. Kober, G. Heinze, and S. A. Kozek-Langenecker, "Electrical stimulation of auricular acupuncture points is more effective than conventional manual auricular acupuncture in chronic cervical pain: a pilot study," *Anesth. Analg.*, vol. 97, no. 5, pp. 1469–1473, Nov. 2003.
[27] S. M. Sator-Katzenschlager, G. Scharbert, S. A. Kozek-Langenecker, J. C. Szeles, G. Finster, A. W. Schiesser, G. Heinze, and H. G. Kress, "The short- and long-term benefit in chronic low back pain through adjuvant electrical versus manual auricular acupuncture," *Anesth. Analg.*, vol. 98, no. 5, pp. 1359–1364, table of contents, May 2004.
[28] T. Payrits, A. Ernst, E. Ladits, H. Pokorny, I. Viragos, and F. Längle, "[Vagal stimulation - a new possibility for conservative treatment of peripheral arterial occlusion disease]," *Zentralblatt Für Chir.*, vol. 136, no. 5, pp. 431–435, Oct. 2011.
[29] S. Fichtenbauer, "Vagus nerve stimulation effects on peripheral perfusion dysfunction in diabetics, Master Thesis, TU Wien." 2014.
[30] K. Takazawa, N. Tanaka, M. Fujita, O. Matsuoka, T. Saiki, M. Aikawa, S. Tamura, and C. Ibukiyama, "Assessment of Vasoactive Agents and Vascular Aging by the Second Derivative of Photoplethysmogram Waveform," *Hypertension*, vol. 32, no. 2, pp. 365–370, Jan. 1998.
[31] L. Wang, L. Xu, S. Feng, M. Q.-H. Meng, and K. Wang, "Multi-Gaussian fitting for pulse waveform using Weighted Least Squares and multi-criteria decision making method," *Comput. Biol. Med.*, vol. 43, no. 11, pp. 1661–1672, Nov. 2013.
[32] U. Rubins, "Finger and ear photoplethysmogram waveform analysis by fitting with Gaussians," *Med. Biol. Eng. Comput.*, vol. 46, no. 12, pp. 1271–1276, Dec. 2008.
[33] D. Goswami, K. Chaudhuri, and J. Mukherjee, "A new two-pulse synthesis model for digital volume pulse signal analysis," *Cardiovasc. Eng. Dordr. Neth.*, vol. 10, no. 3, pp. 109–117, Sep. 2010.
[34] E. Kaniusas, *Biomedical Signals and Sensors II: Linking Acoustic and Optic Biosignals and Biomedical Sensors*. Springer, 2015.

[35] T. O'Haver, "Interactive Peak Fitter." [Online]. Available: http://terpconnect.umd.edu/~toh/spectrum/InteractivePeakFitter.htm. [Accessed: 02-Jun-2015].
[36] "PWV Analysis Parameters - QHRV." [Online]. Available: http://www.qhrv.es/dtr_pwv_parameters.htm. [Accessed: 02-Jun-2015].
[37] L. Gbaoui and E. Kaniusas, "Arterial pulse wave decomposition by independent component analysis," in *IEEE International Workshop on Medical Measurements and Applications, 2009. MeMeA 2009*, 2009, pp. 111–115.
[38] S. S. DeLoach and R. R. Townsend, "Vascular Stiffness: Its Measurement and Significance for Epidemiologic and Outcome Studies," *Clin. J. Am. Soc. Nephrol.*, vol. 3, no. 1, pp. 184–192, Jan. 2008.